



Imaging the Crustal Structure Throughout the East Anatolian Fault Zone, Turkey, by Local Earthquake Tomography

CAGLAR OZER,^{1,2}  MEHMET OZYAZICIOGLU,^{1,2} ELCIN GOK,³ and ORHAN POLAT³

Abstract—This paper presents new models of the seismic velocity structure of Eastern Anatolia, Turkey. We applied a local earthquake tomography method to arrival time data produced by local and regional events in Eastern Anatolia to understand the three-dimensional seismic velocity and V_p/V_s models and their correlation with the geological evolution and tectonic processes in the study area. The data are obtained from 78 broadband seismic stations, owned by the Earthquake Department of the Disaster and Emergency Management Presidency, for the period between 2008 and 2017. Seven depth cross sections are taken along various segments of the East Anatolian Fault Zone. Travel times of 53,099 phase readings (29,122 P-phase and 23,977 S-phase picks) from 4249 high-quality earthquake recordings are analysed to develop 3-D V_p (lithological) and V_p/V_s (petrological) models of the study area. The resulting P-wave velocities describe intrusive magmatic bodies, sediment thickness and the structure of the basin. The V_p/V_s structures aid to limit the position of the faults, areas of weakness, and gas- or liquid-saturated units with regions of high pore pressure. Four main seismic crustal layers down to 40 km are determined. The upper crust (0–8 km) has $V_p \leq 4.6$ km/s, whereas in the middle crust (~ 9 –20 km) a V_p perturbation between 4.6 and 5.8 km/s is observed. In the lower crust (~ 20 –35 km), V_p changes from 5.9 to 7.3 km/s and in the upper mantle layer (below 36 km), V_p exceeds 7.4 km/s. In all cases, seismic velocities are well-resolved in the first 40 km. Tomograms are compatible with the geological characteristics of the region. Dominant high P-velocity values are observed beneath the collision zone. Conrad discontinuity is detectable at 20 km depth, while Moho depth is observed to vary between 30 and 40 km in the study area.

Key words: Local earthquake tomography, crustal structure, seismic velocity, East Anatolia fault zone.

1. Introduction

Turkey is mainly located in the Alpine-Himalayan orogenic belt. The seismic activity of the Eastern Anatolian Region results from the convergence of the Eurasian, African and Arabian plates (McKenzie 1972, 1976; Dewey et al. 1986; Jackson 1994; Le Pichon et al. 1995; Sengor and Natal'in 1996; McClusky et al. 2000; Gok et al. 2011; Delph et al. 2015). The Arabian plate is moving in a north-northeast direction with respect to Eurasia at a rate of about 15 mm/year. This northward migration of the Arabian plate results in continental collision along the Bitlis Suture Zone (BSZ) and Zagros Belt. (Hempton et al. 1981; Hempton 1985, 1987; Sandvol et al. (2003); Dolmaz et al. 2008; Aktug et al. 2016) (Fig. 1). The northward motion of the African plate exhibits a plunge in the oceanic lithosphere beneath the Anatolian plate along the Aegean-Cyprian Arc (Le Pichon and Kreemer 2010; Reilinger et al. 2006; Walters et al. 2014; Simao et al. 2016). Tectonic, seismologic and geodetic studies divide the region into three main geodynamic regions: a strike-slip regime in the north and northwest along the North Anatolian Fault Zone (NAFZ), a N–S extension in the west (Aegean region), and a strike-slip deformation in the east of Turkey, particularly along the East Anatolian Fault Zone (EAFZ) (Burke and Sengor 1986; Nalbant et al. 2002; GURSOY et al. 2003; Orgulu et al. 2003; Vanacore et al. 2013; Simao et al. 2016). The EAFZ is a 550 km-long fault zone extending between Karliova in the northeast and Antakya in the southwest. It is an approximately northeast-trending, left-lateral strike-slip fault zone (Fig. 2) consisting of a number of segments (Perincek and Cemen 1990;

¹ Earthquake Research Centre, Ataturk University, 25240 Erzurum, Turkey. E-mail: caglaroz@atauni.edu.tr

² Department of Civil Engineering, Engineering Faculty, Ataturk University, 25240 Erzurum, Turkey.

³ Department of Geophysics, Engineering Faculty, Dokuz Eylul University, 35160 Izmir, Turkey.

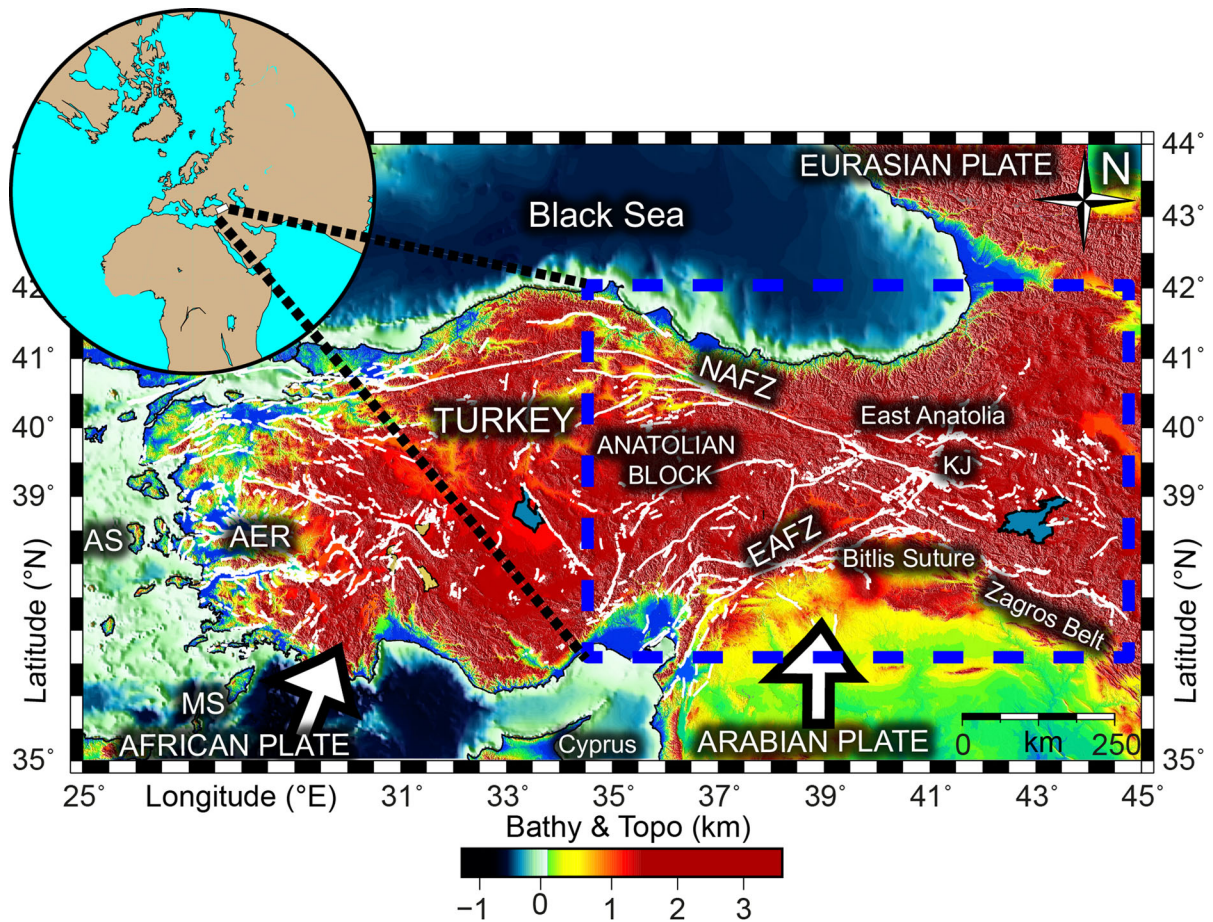


Figure 1

Tectonic settings of Anatolia. Blue dashed line represents the study area. AER Aegean extensional regime, AS Aegean Sea, EAFZ East Anatolian Fault Zone, KJ Karliova Junction, MS Mediterranean Sea, NAFZ North Anatolian Fault Zone (compiled from Emre et al. 2013; Bartol and Govers 2014)

Saroglu et al. 1992; Aksu et al. 1992; Italiano et al. 2013).

The main fault segments of the EAFZ from SW to NE are as follows: Antakya-Turkoglu, Turkoglu-Golbasi, Golbasi-Celikhan, Sincik-Hazar, Hazar-Palu and Bingol-Karliova, respectively (Italiano et al. 2013). Earthquakes of varying magnitude throughout the EAFZ indicate ongoing tectonic activity. The Antakya-Turkoglu segment (Fig. 3a) has a left-lateral fault structure accompanied with an eastward dip-slip component. This segment is generally not straight (Ergin et al. 2004; Duman and Emre 2013). According to focal mechanism solutions, Turkoglu-Golbasi segment (Fig. 3b) is a left-lateral strike-slip fault with a slight dip-slip component (Kop et al.

2014). The length of the segment is ~ 30 km and filled with sediments. The Golbasi-Celikhan segment (Fig. 3c) consists of ~ 20 km sub-segments with active left-lateral strike-slip characteristics. The drainage connection is offset by a few meters to 0.5 km within Holocene-age sediments (Duman and Emre 2013). The Sincik-Hazar segment (Fig. 3d) is separated from the Hazar-Palu segment by Hazar Lake, which was interpreted as a pull-apart basin (Cetin et al. 2003). Due to its complex structure at the extremities, the Hazar-Palu segment (Fig. 3e) is separated into three parts. The Bingol-Karliova segment (Fig. 3f) starts at the junction of the NAFZ and the EAFZ, which is known to be the Karliova

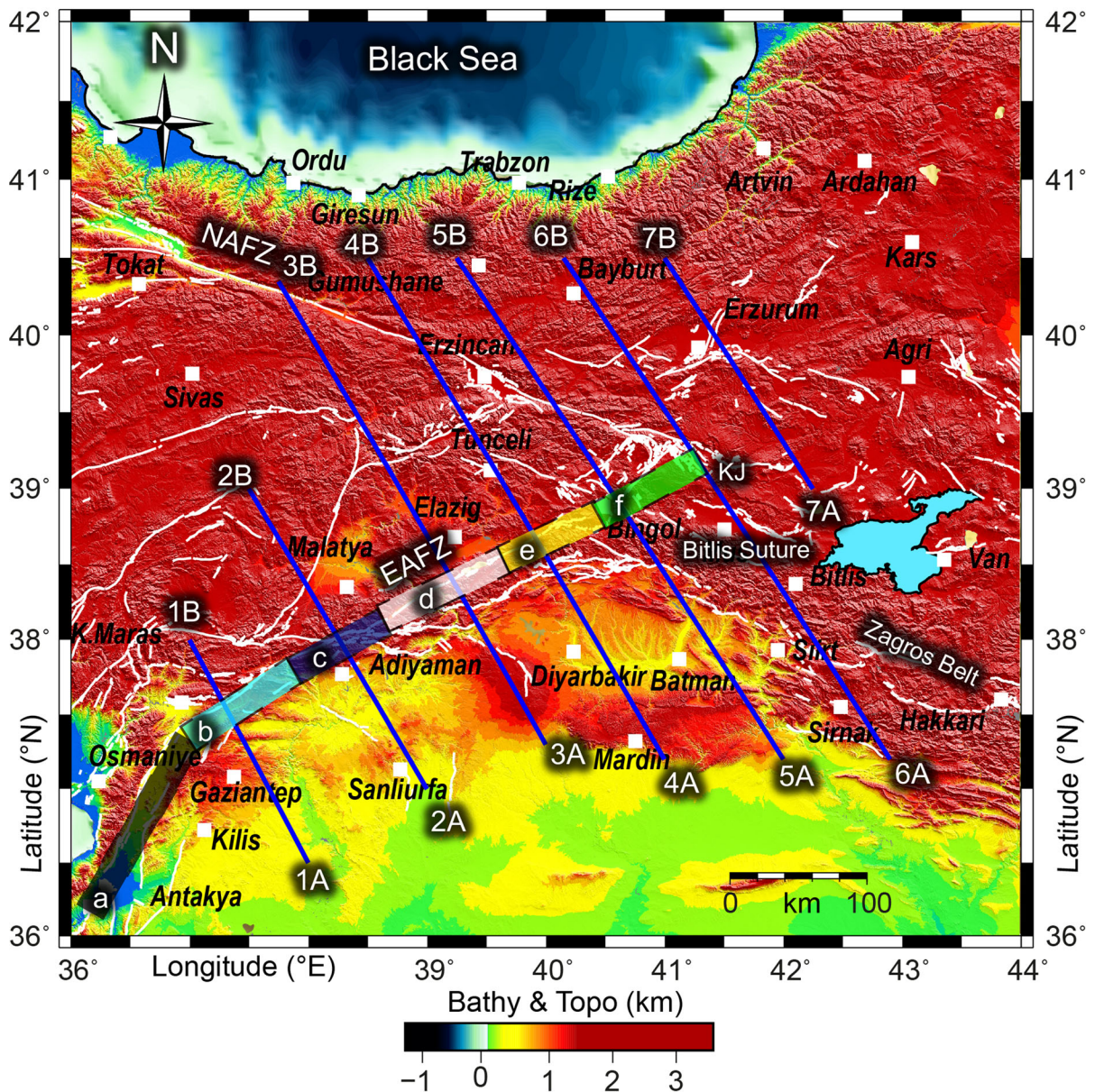


Figure 2

Topography and main tectonic units for a large area of Eastern Anatolia. Blue and white lines show the location of profiles and main fault zone, respectively. (a) Antakya-Turkoglu segment, (b) Turkoglu-Golbasi segment, (c) Golbasi-Celikhan segment, (d) Sincik-Hazar segment, (e) Hazar-Palu segment and (f) Bingol-Karllova segment. *EAFZ* East Anatolian Fault Zone, *KJ* Karllova Junction, *NAFZ* North Anatolian Fault Zone (compiled from Emre et al. 2013; Italiano et al. 2013)

Junction (KJ). This segment comprises right-stepping sections ranging in length from 4 to 12 km.

Several geophysical studies of seismic activity have been conducted in Eastern Anatolia. Gok et al. (2003) noted an increasing depth of the Moho, from 34 to 52 km, in a south-to-north direction in Eastern

Anatolia. Using the receiver function method and a set of teleseismic events from the temporary PASS-CAL network of 29 seismometers, Zor et al. (2003) determined a crustal thickness and an average S-wave velocity of 45 km and 3.7 km/s, respectively, for the Eastern Anatolian Plateau. Sandvol et al. (2003)

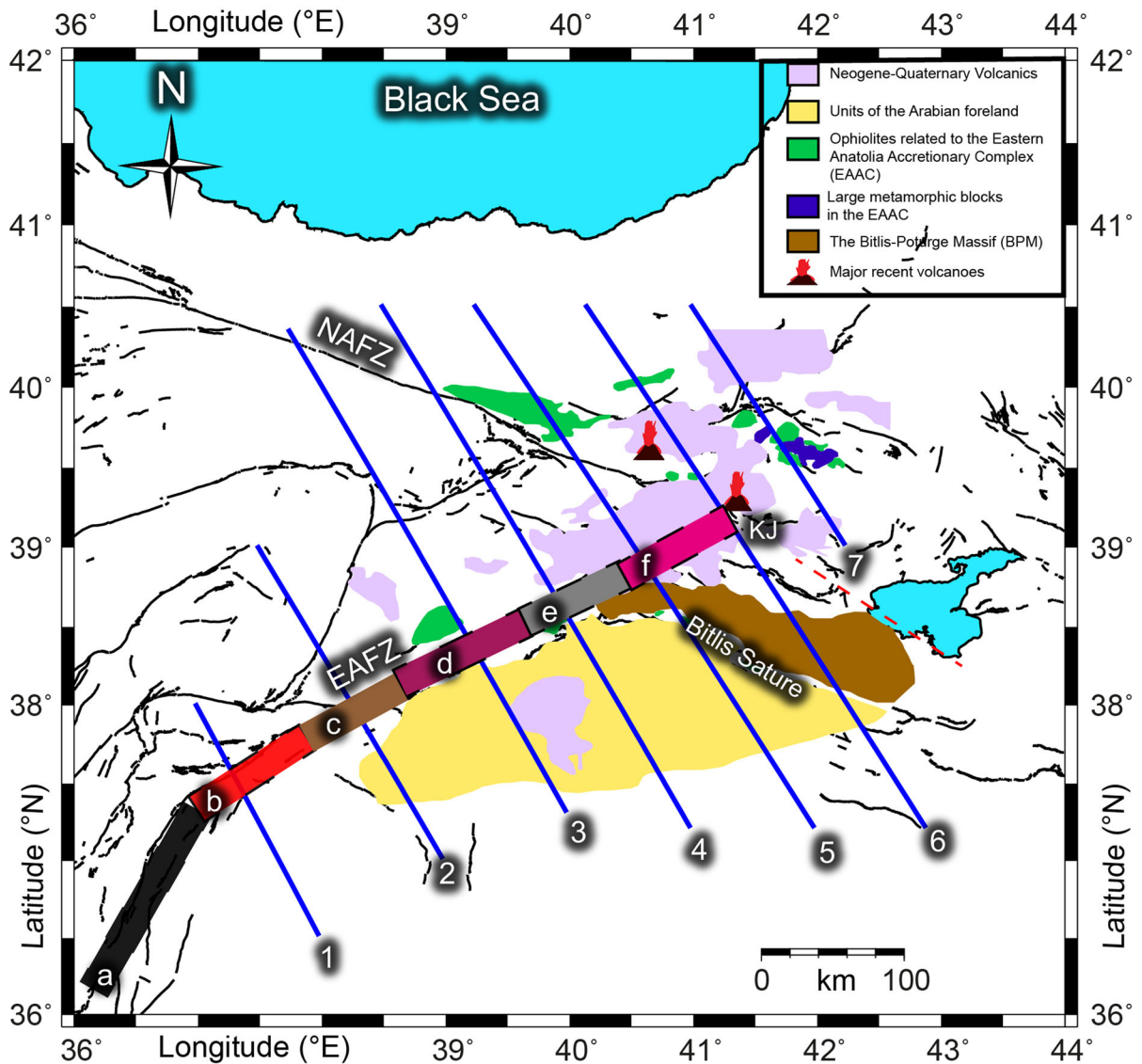


Figure 3

Main geological map of Eastern Anatolia, Turkey (compiled from Emre et al. 2013; Italiano et al. 2013). (a) Turkoglu Antakya segment, (b) Turkoglu-Golbasi segment, (c) Golbasi-Celikhan segment, (d) Sincik-Hazar segment, (e) Hazar-Palu segment and (f) Bingol-Karlioiva segment. EAAC Eastern Anatolia Accretionary Complex, EAFZ East Anatolian Fault Zone, KJ Karlioiva Junction, NAFZ North Anatolian Fault Zone

revealed the structure of the Bitlis/Zagros zones and the EAFZ and NAFZ using the PASSCAL network to image the upper mantle and crustal structure scope of the Eastern Turkey Seismic Experiment (ETSE) project. Kaypak and Eyidogan (2005) found evidence of an approximately 2 km-thick sedimentary cover in the Erzinca basin with very low P-wave velocity as well as a crustal structure characterized by a low V_p/V_s

ratio throughout Eastern Anatolia. Gok et al. (2008) reported crustal thickness of 38 km for Mardin in a study using receiver function analysis carried out in Iraq and its surroundings. Ozacar et al. (2008) calculated crust and lithosphere thickness of 40 and 65 km, respectively. Zor (2008) proposed that negative velocity perturbation at 200 km could indicate a partially molten asthenosphere. The region is also

identified by low seismic velocities, as demonstrated by Mutlu and Karabulut (2011), while Salah et al. (2011) showed that the low-velocity values of P- and S-waves imply partial melting of the upper mantle. Gokalp (2012) imaged the crust beneath Eastern Anatolia using the local earthquake tomography method. Sertcelik (2012) investigated the EAFZ using the coda wave attenuation method to show attenuation changes at different segments. Bektas (2013) reported Curie point depths of Eastern Anatolia ranging from approximately 16 to 19 km using aeromagnetic and gravity data. Warren et al. (2013) imaged high velocity at 20 km that may be associated with the underthrusting Arabian Plate in the south-eastern part of Turkey. Skolbeltsyn et al. (2014) asserted that the high-velocity areas beneath the eastern Caucasus and Kura region were associated with ongoing subduction. Maden et al. (2015) calculated average sedimentary thickness, Moho and Conrad depths of 5.2, 43.0 and 20.9 km, respectively, in the Erzurum area, Eastern Anatolia.

Local earthquake tomography (LET) is a suitable technique for examining the tectonics and seismogenic properties of a region (Ozer and Polat 2017a, b, c; Ozer et al. 2018). Seismic velocity changes in the crust are generally associated with lithological units, petrological features and tectonic variations. The calculated seismic images obtained by the LET method provide an understanding of the relationships of shallow to deep tectonic characteristics, weakness zones and changes in seismic characteristics in the crust related to geological features (Gentile et al. 2000). The main purpose of the current study is to use arrival time knowledge to calculate V_p and the V_p/V_s ratio characteristics for the crust beneath the EAFZ and to reconcile them with the tectonics based on previous geological and geophysical studies in the region. Such analysis can also reveal the structure of tectonic processes and geological units the region has experienced from past to present (Kaypak 2008; Salah 2014).

In this study, we apply the LET method to evaluate crustal thickness variations in Eastern Anatolia. The P-velocity and V_p/V_s ratio changes in the crust are generally associated with the lithological and tectonic units as well as petrological characteristic of rocks, such as faults or rich fluid content and high-

pore-pressure zones. We present 3-D models of seismic velocity structure V_p and V_p/V_s for the crust in Eastern Anatolia. We used regional event data recorded between 2008 and 2017 by the Turkish National Seismic Network of the Earthquake Department of Disaster and Emergency Management Presidency (AFAD); the network description, operation and use of data can be found elsewhere (Kilic et al. 2017). The distribution of seismic stations and events is shown in Fig. 4. During this period, 48,106 events in Eastern Anatolia were recorded in the network and located using a preliminary seismic velocity model (Table 1) (Maden 2012). We suggest a new seismic crustal model to better reflect the collisional deformation at the upper crustal layer. The results of this study facilitate our understanding of continental collision processes and the rheological characteristics of the crust. Thus, although the seismic velocity model covers the entire subduction zone, the discussion of the results in this paper will focus on those parts in the Eastern Anatolian Region that are new and have not been analysed before.

2. Data, Algorithm and Checkerboard Test

We used arrival times recorded by permanent three-component broadband seismic stations in an area of about $8^\circ \times 5^\circ$ in Eastern Anatolia. A total of 48,106 regional earthquakes ($M_L \geq 2.0$) were recorded over a period of 9 years by 78 seismic recorders in the region located between the coordinates $36\text{--}42^\circ\text{N}$ and $36\text{--}44^\circ\text{E}$, covering the collision zone of the Arabian and Eurasian plates. The events picked by AFAD were selected according to the following criteria: a minimum of ten P-phase arrivals, with a clear onset per earthquake and an RMS smaller than 0.3 s; in addition, an earthquake was discarded if the horizontal distance to the nearest instrument exceeded 500 km. There were 4249 events determined to satisfy these criteria, with 29,122 P- and 23,977 S-wave arrival times. The average accuracy of the final P- and S-travel time residuals were 0.28 and 0.41 s, respectively, after five iterations (Table 2). In general, the $V_p\text{--}V_p/V_s$ inversion technique leads to larger RMS values than the $V_p\text{--}V_s$ scheme. However, this situation does not imply that the older method

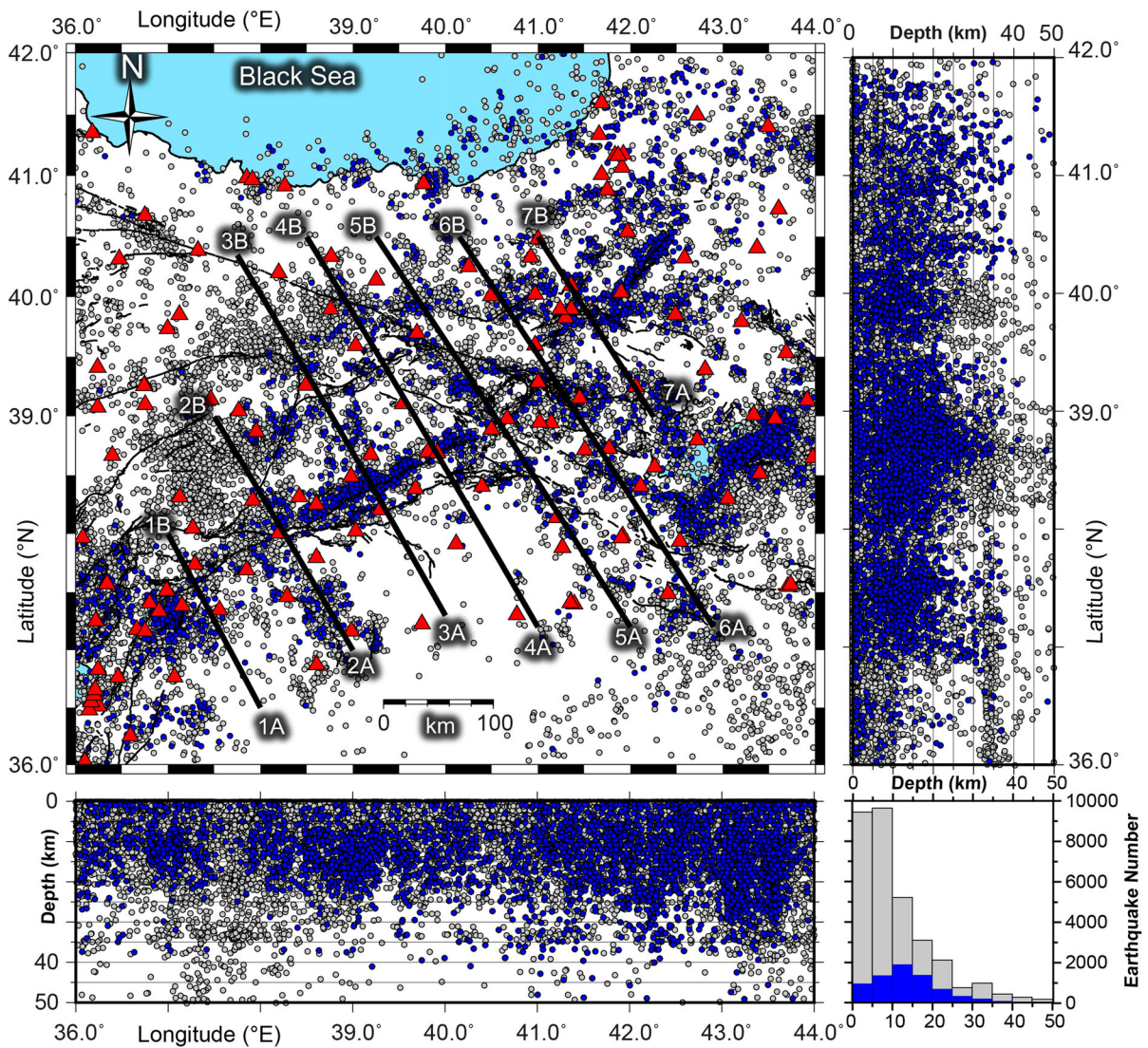


Figure 4

Locations of initial 48,106 (gray) and selected 4249 (blue) events (hand-picked, $M \geq 2.0$) recorded between 2008 and 2017 in Eastern Anatolia. Stations, initial earthquakes and selected events are represented by filled red triangles, gray circles and blue circles, respectively. Thin black lines show fault traces (digitized after Emre et al. 2013). Events are mainly located in the first 40 km depth of the crust, as is clearly visible from vertical sections and the histogram which displays the number of events versus depth

Table 1

Reference model for P velocity (Maden 2012)

Depth (km)	P-wave velocity (km/s)
0.0	4.4
4.0	5.8
20.0	6.2
35.0	7.1
50.0	8.0

provides a poorer solution than the latter, taking into consideration that the inversion process for $V_p - V_p/V_s$ provides minimization of differential P-S residuals, while the $V_p - V_s$ scheme minimizes the P and S residuals separately, which are accounted for in the reported RMS (Koulakov et al. 2010).

The LET has been used to compute the seismic velocity structure of the Earth's crust and uppermost

Table 2

RMS (s) values of the P- and S-wave residuals after five iterations for V_p and V_s inversion procedures

Iteration	RMS P (s)	RMS S (s)	Reduction P (%)	Reduction S (%)
1	0.41	0.68	–	–
2	0.36	0.48	12	28
3	0.34	0.45	16	32
4	0.30	0.43	20	35
5	0.28	0.41	24	37

mantle at local or regional scales (from the surface to 100 km) (Serrano et al. 2002; Gokalp 2007, 2012; Koulakov et al. 2009; Dinc et al. 2010; Jaxybulatov et al. 2011; Kaypak and Gokkaya 2012; Totaro et al. 2014). Because there is a trade-off between the earthquake location and origin time and the seismic velocity structure, these data are solved simultaneously. We use a popular LET algorithm, LOTOS-12 (Koulakov 2009), for simultaneous inversion of V_p - V_p/V_s structure and hypocentral parameters. The LOTOS algorithm can be used with very different data sets and has a user-friendly interface. Based on Maden (2012), we formed an initial 1-D seismic velocity model (Maden 2012) (Table 1). The algorithm starts with preliminary earthquake locations and an initial 1-D seismic velocity model. In this part of the analysis, earthquake origin times and source coordinates are obtained by a grid search method (Koulakov and Sobolev 2006). The main aspect of this method is the goal function (GF), which indicates the contingency of earthquake location in the 3-D model space. At the first stage, the travel times are considered the same as in the 1-D velocity model; this feature speeds up location computations. Then the earthquake locations in the 1-D velocity model are corrected iteratively in the simultaneous inversion step for 1-D velocities, source coordinates and origin times. After the optimization of the final 1-D seismic velocity model, the sources are relocated by the 3-D velocity model. In this stage, two options are available in the LOTOS-12 code to parameterize the velocity profile: (1) with cells and (2) with nodes. In this study, the node parameterization method is used for modelling the area. We also used several grids with different orientations (0° , 22° , 45° and 67°) in

order to decrease any grid dependency by averaging the results.

The inversion process may also be controlled by the amplitude and smoothness matrix block. The weight of this regulator matrix can improve the inversion results dramatically. With these special matrices, source correction and other free parameters can be determined using synthetic tests (Koulakov 2009; Koulakov et al. 2010; Khrepy et al. 2015). The inversion algorithm used in P velocity and the V_p/V_s ratio is described extensively in Wagner et al. (2007). The LSQR algorithm used in the matrix inversion is described in detail in Paige and Saunders (1982).

The synthetic test in LOTOS allows us not only to determine the best values for the free inversion parameters, such as amplitude damping, smoothing factor and weight factor, but also to determine the resolution of the model, which may then be used to improve the inversion with real data. We tried several synthetic and computed data to achieve the optimal values for free parameters. The synthetic travel times are calculated by a bending ray tracing algorithm which is characterized by alternating positive and negative velocity anomalies. In addition, a large part of the study area is adequately covered in terms of ray traces, with a plethora of ray paths along and across the EAFZ (Fig. 5).

The noise in the synthetic data set is created by random values of histogram type residuals. The average amplitude of noise is taken as 0.28 s and 0.41 s for P- and S-waves, respectively. Initial residual values of the largest 1.0 s travel time were found to fall below 0.5 s after the inversion process (Fig. 6). The initial models of all synthetic tests are formed using node parameterization.

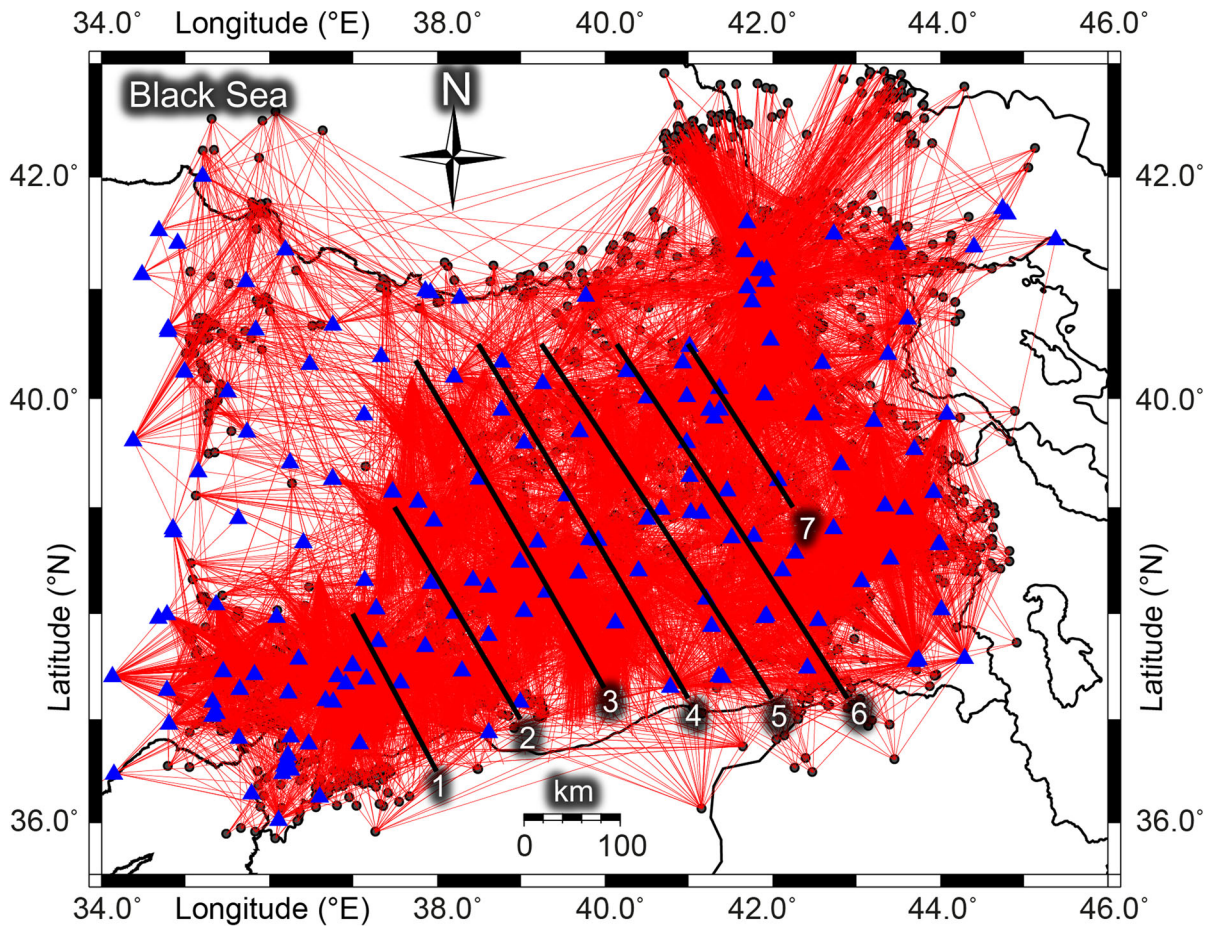


Figure 5

Horizontal ray path coverage of P-wave data set in plain perspective. Straight red lines show the pathway between earthquakes (black circles) and seismic stations (blue triangles). Black lines display the locations of profiles

In this study, the velocity model produced by Maden (2012) was used as a 1-D seismic velocity model. The four prominent seismic velocity models reported for the study area were tested as an input model; they were compared with the LOTOS 1-D velocity optimization results, and the best model that converged to them was selected. It is clearly seen that the 1-D seismic model produced by Maden (2012) coincides and converges with the data set (Fig. 7a). A velocity model reported by Teoman et al. (2005) is the second best model to represent the study area. However, a mismatch was observed in this model, especially after a depth of 10 km (Fig. 7b). In addition, the calculated RMS values were higher in the velocity models reported by Salah et al. (2011)

(Fig. 7c) and Gokalp (2012) (Fig. 7d), which is thought to be related to model uniformity.

Figure 8 illustrates the final reconstruction of the checkerboard models defined for all even and odd data sets. The size of anomalies is $50 \times 50 \text{ km}^2$ in all models and the values of anomalies in all cases are $\pm 10\%$, periodically.

In order to determine the effect of noise on the resolution and the optimal values of free parameters, we conducted various synthetic tests. When conducting the checkerboard tests, a solution is accepted when neither the earthquake location nor the initial 1-D seismic velocity model is known previously. A successful synthetic checkerboard test shows which part of the model can be solved better, sufficiency of

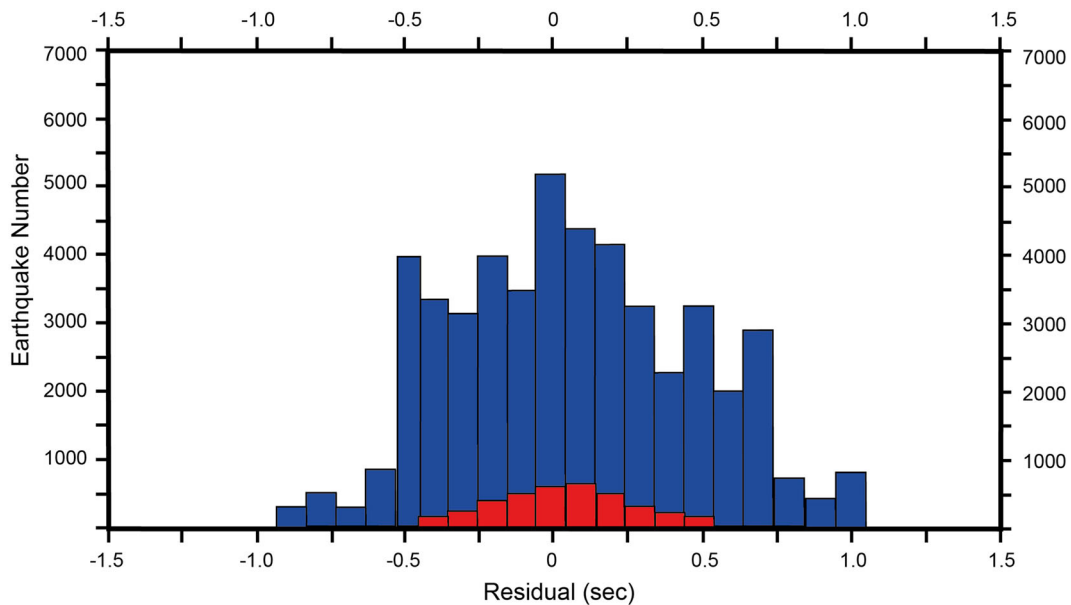


Figure 6
Initial (blue) and final (red) travel time residual values of earthquakes

station and event coverage. The artificial travel times are computed for source-receiver pairs in the same way as for the real observed data. The source locations of real events are fixed after five iterations in order to calculate unknown parameters more accurately. The synthetic data consist of random noise, giving the same variance reduction as in the real data inversion case. At the end of synthetic data processing, we disregard all source and velocity model information and start to rebuild using the same operation and inversion parameters as in the real data processing. These tests can be used to determine the well-resolved part of the study area, and also give an idea about the values to be adopted for free inversion parameters in tomography. In this study, the checkerboard test showed that the data were able to successfully resolve almost the entire central part of Eastern Anatolia between 37.5–40.5°N and 37.0–43.0°E and its near surroundings down to about 40 km (Fig. 8).

The even/odd synthetic tests show the effect of noise in the data. The travel time catalog is randomly subdivided into two parts according to event numbers, and the effect of noise on the final results can be predicted using these tests. For instance, in our study,

the results of the even tests are similar to those of the odd tests up to a depth of 10 km, while 20, 30 and 40 km horizontal cross-section anomalies in the central part of the study area look similar to each other. However, in the horizontal section at the surface, model reconstruction is not correct, because surficial event sources do not exist in the data. The even/odd and the checkerboard test results demonstrate whether the outcomes are robust and unaffected by other factors (Fig. 8). The major characteristics discussed here are obvious in all cases, indicating that our model is rather robust by all tests (Koulakov 2009; Koulakov et al. 2010; Jaxybulatov et al. 2011; Totaro et al. 2014; Khrepy et al. 2015). Furthermore, to be able to prove the adequacy of horizontal ray distribution in the study area, we used fine grid spacing (5 km) in a lateral section at the central part of the model, which has a high ray density, especially along the EAFZ (Fig. 5). Therefore, the good ray coverage displayed in most cross sections of eastern Turkey shows the reliability of the computed wave velocity and thus the V_p/V_s ratio based on the data set used in this research (Fig. 8).

In order to better understand the resolution in the study area, 25×25 km horizontal (Fig. 9) and

30 × 30 km (with 5 km gap) vertical checkerboard tests were conducted for V_p (Fig. 10) and V_p/V_s (Fig. 11) models along with even/odd tests constituted by 50 × 50 km cubes. As a result of all these tests, the areas where the resolution of the tomographic model was high are determined. In the horizontal checkerboard model, the resolution is very poor in the southern part of the working area. This poor resolution along the Syrian border is due to the sparse station distribution and the resulting decreased ray intensity. A similar situation is observed along the Black Sea coastline in the north. The checkerboard test results show that the resolution gradually decreases from 0 to 40 km. However, the resolution is still satisfactory, as can be seen in the horizontal sections of 40 km. Therefore, the horizontal sections

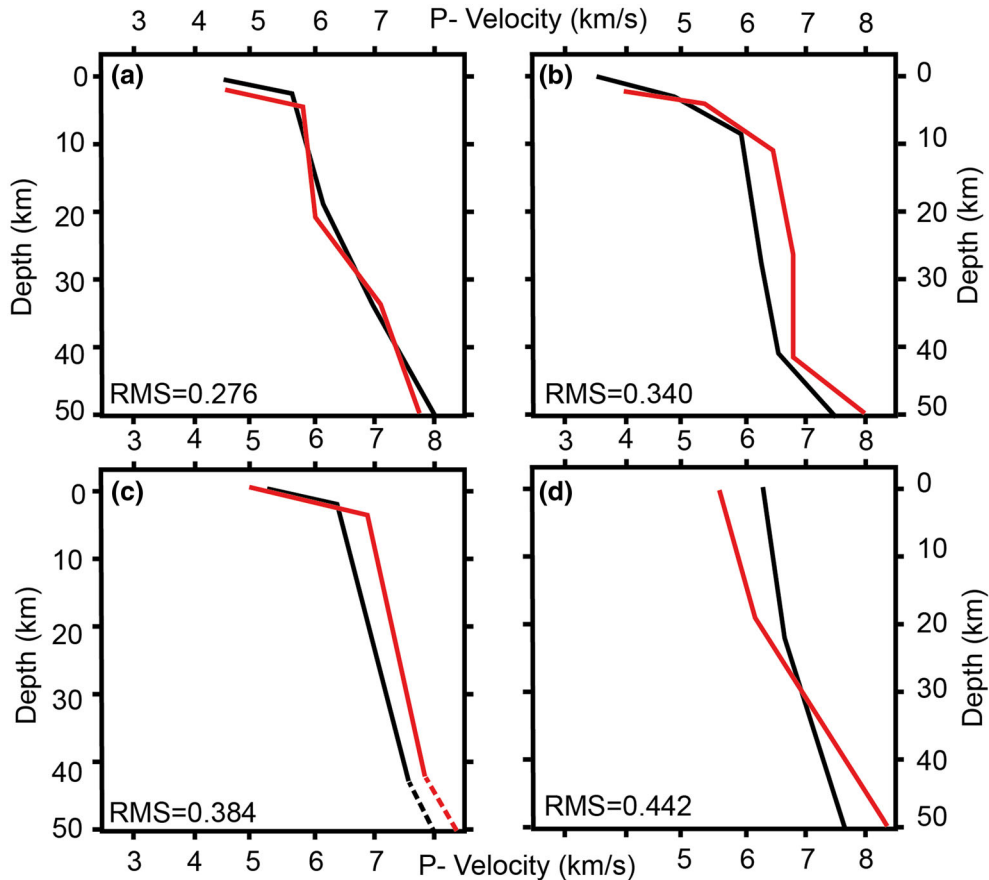


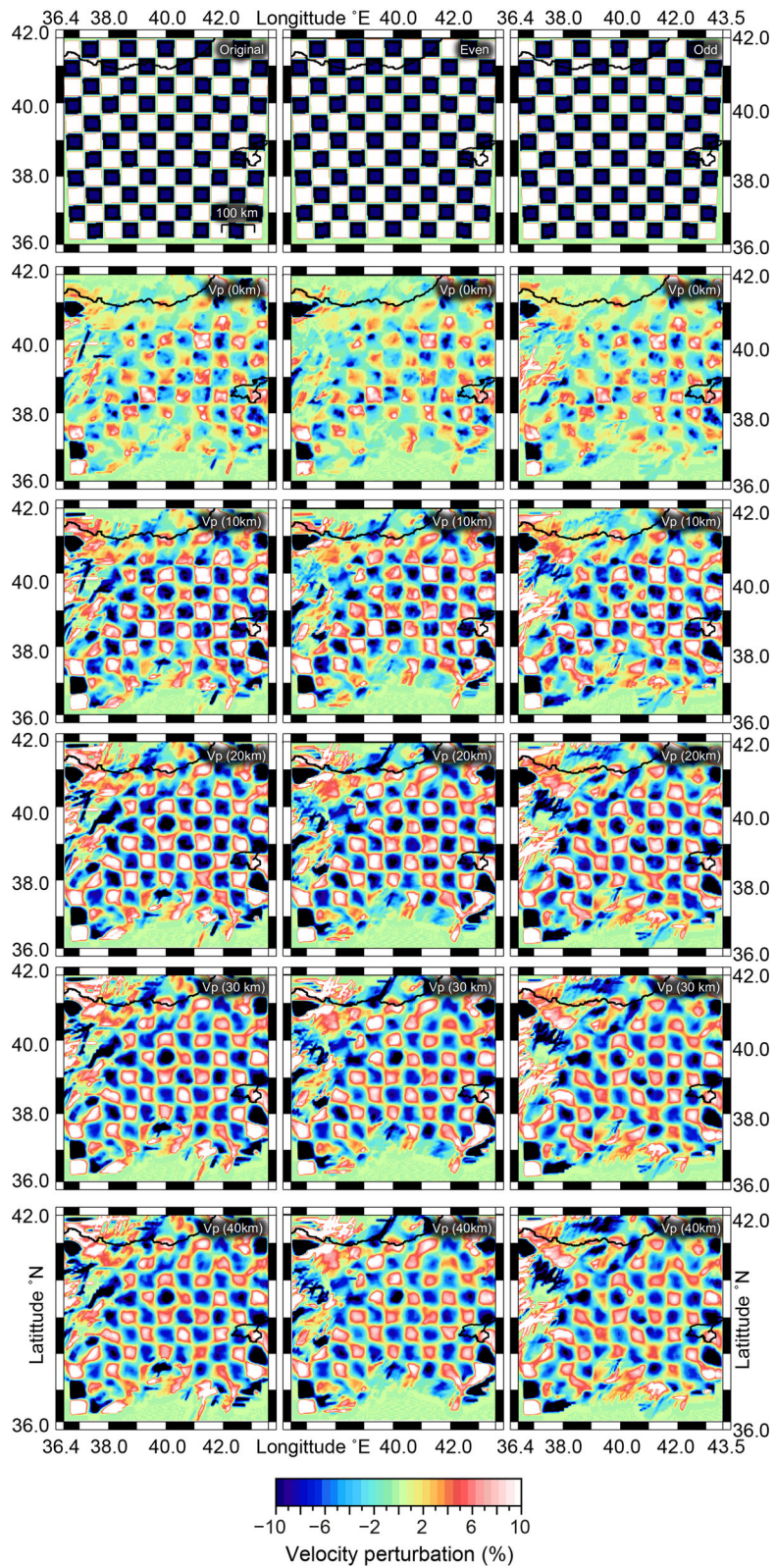
Figure 7

1-D seismic velocity model optimization results produced using the different seismic models. Initial and final models are represented by black and red lines, respectively. The 1-D seismic velocity models used as initial models in this study are **a** Maden (2012), **b** Teoman et al. (2005), **c** Salah et al. (2011), and **d** Gokalp (2012)

Figure 8

Horizontal checkerboard test results obtained for P-wave travel times to predict the optimal values of inversion parameters down to 40 km depth layers with unlimited vertical columns. Periodic negative (blue) and positive (red) anomalies display $\pm 10\%$ velocity perturbations for 50 km box size. The input for each model is given at the top of each column. Synthetic (checkerboard) tests (left column) are applied to determine the resolution capacity of the model. Even/odd test results of the inversion of two independent data subsets down to 40 km are presented in the middle and right columns, respectively

in this study were interpreted as reliable up to a depth of 40 km. In order to precisely interpret the seismic vertical models, a checkerboard test was used for V_p and V_p/V_s sections, and the areas where the resolution was high were determined (Figs. 10, 11). According



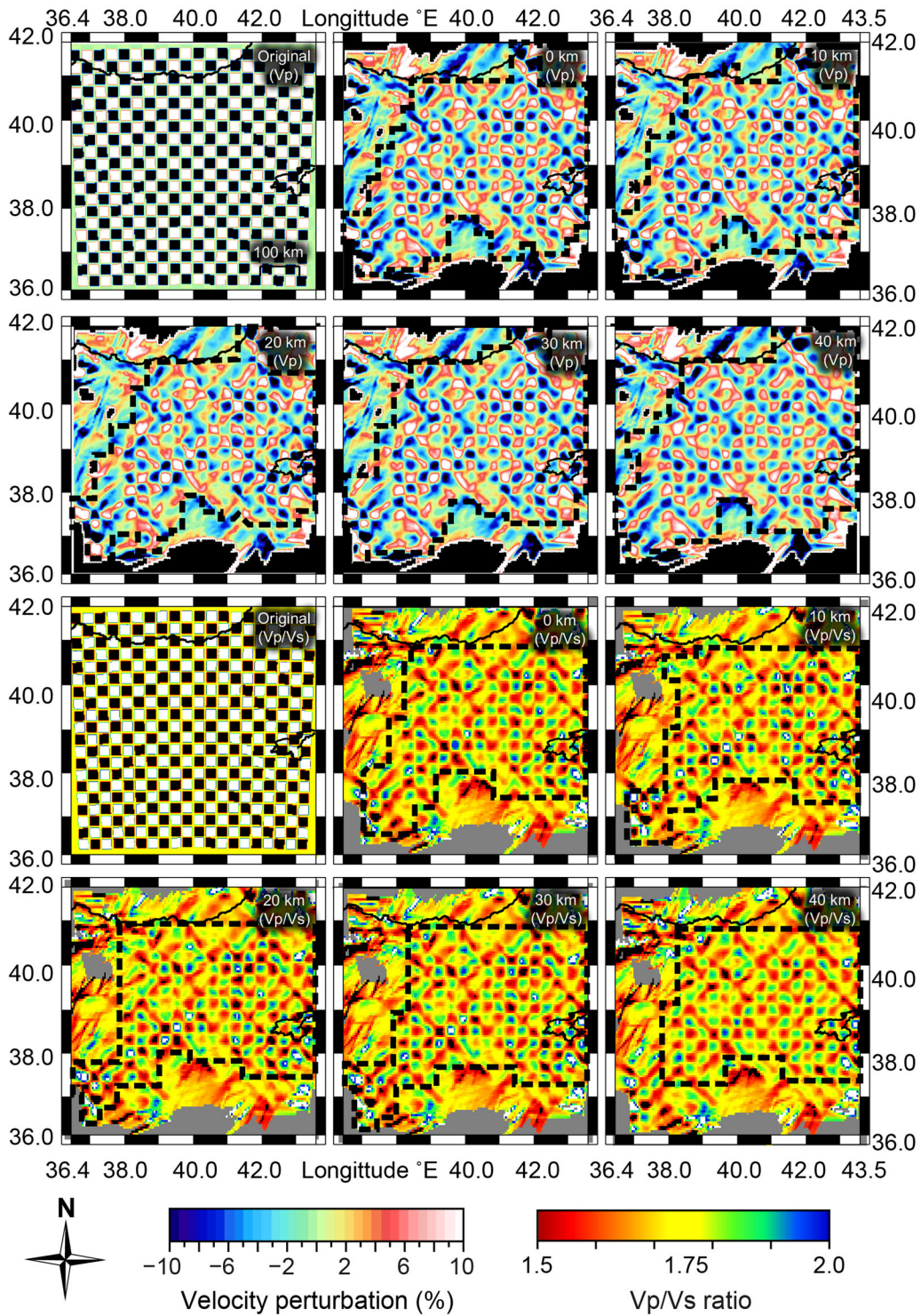


Figure 9

Horizontal checkerboard test results for $25 \times 25 \text{ km}^2$ box size with unlimited vertical columns. Anomalies change $\pm 10\%$ for P-wave velocities. V_p/V_s ratio ranges from 1.5 to 2.0. The dashed lines indicate well-resolved areas

to these results, the resolution decreases slightly in the last 20 km of profile 1 and in the middle parts of profile 6. V_p and V_p/V_s vertical checkerboard test results show that all vertical sections can be reliably interpreted. The vertical profile locations designed by taking into consideration the ray intensity, seismic station geometry and earthquake distributions are sufficient to reveal the tectonic structure of the EAFZ (Figs. 10, 11).

3. Tomographic Results

3.1. Horizontal Tomographic Results

The horizontal sections obtained up to a depth of 40 km reveal a $\pm 10\%$ velocity change for the P-wave inversion. Black dashed lines show the area at high resolution (Fig. 12). The positive P-wave velocity change along the EAFZ is remarkable in the 0 km horizontal depth section. These observed high velocities are very similar to those of Neogene-Quaternary volcanic and ophiolite unit distribution geometry (Italiano et al. 2013). The similar velocity structure continues increasingly in the 10 km depth layer. In addition, the low velocities between 2 and 4 km reported by Gok et al. (2007) are clearly traceable on the 10 km section. Gok et al. (2011) point out the seismic velocities which are relatively homogenous at the horizontal shear wave sections and decrease as the depth increases. In this study, the negative velocity changes started after 20 km depth and continued down to 40 km. Gok et al. (2007) reported very low shear wave velocities from 30 to 38 km in the Northeast Anatolia Plateau. Furthermore, they stated that the Love wave velocities continue down from 10 to 40 km. In addition, the ETSE project result showed that the crustal thickness continues up to 48 km. By interpreting attenuation and tomographic studies together, Gok et al. (2007) concluded that the Eastern Anatolian Plateau lacks the mantle lithosphere, which is associated with the fracture of the wracked part towards the north and the melting of lower levels of volcanism. The Anatolian Plateau crust is not as thick due to contact with the hot atmosphere as a result of volcanism (Sandvol et al. 2003; Gok et al. 2011; Bartol and Govers 2014). The low velocities reported

to be more than 20 km deep in previous studies (Gok et al. 2007, 2011; Warren et al. 2013; Skolbeltsyn et al. 2014) were also observed in horizontal tomographic sections. These negative changes traced in deeper layers are thought to be caused by the hot mantle effect associated with volcanism as noted by Sandvol et al. (2003) and Gok et al. (2011) (Fig. 12).

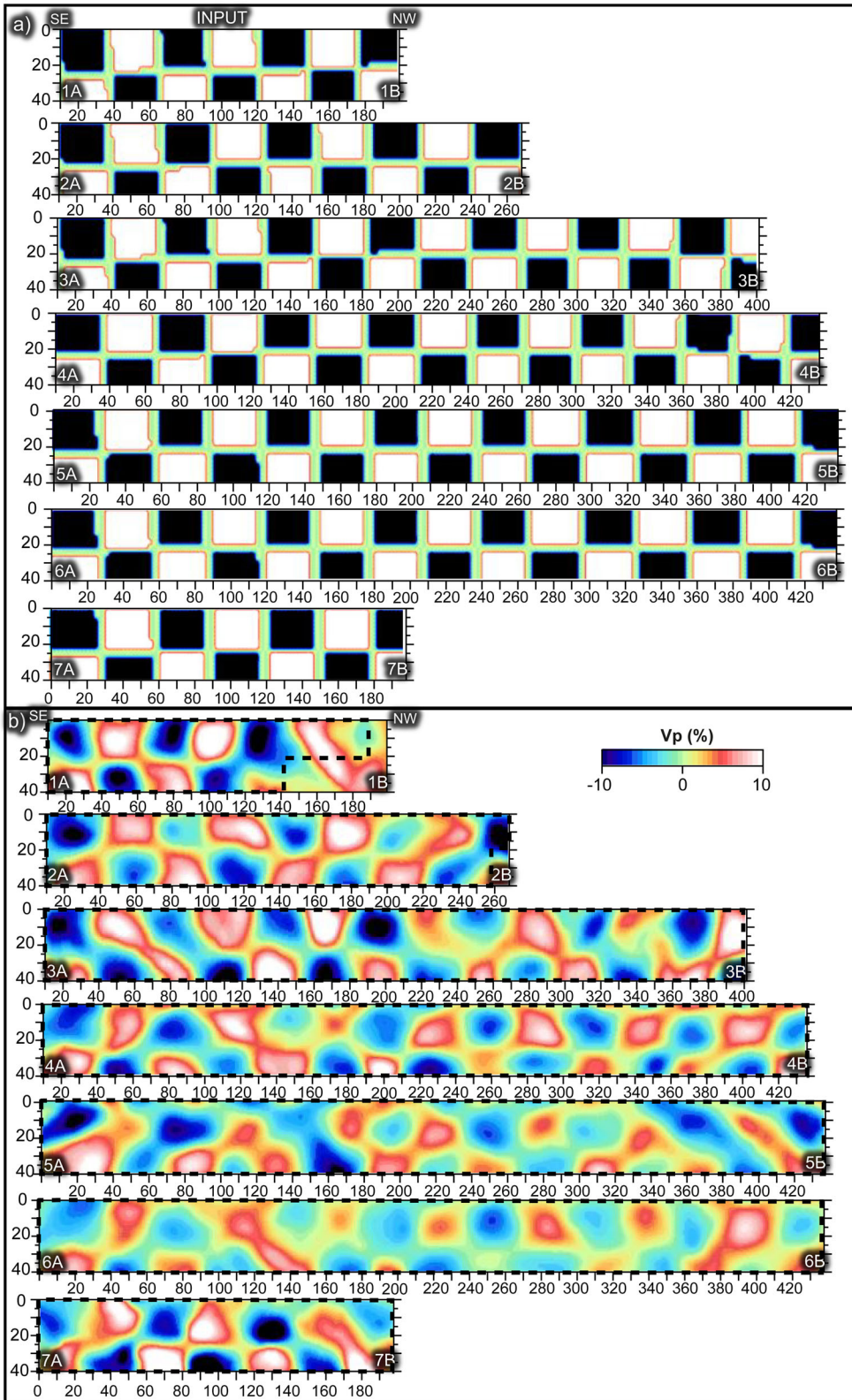
3.2. Vertical Tomographic Results

The tomographic inversion results for P-wave velocity and V_p/V_s ratio profiles at seven parallel vertical cross sections are shown in Figs. 13 and 14, respectively. The absolute velocity distribution indicates a nearly horizontal layering, and the tomogram shows good correlation with the known tectonic and geological characteristics of the study area. Our tomographic models illustrate P-wave velocities that vary from 3.0 to 9.0 km/s, from the surface to crustal depth of 40 km. It is observed that in most of the vertical velocity profiles, the P-wave velocity image characteristics are very similar. Some variations can be explained by the complex geological structures and the active tectonics of the upper crust. The crust beneath Eastern Anatolia is under a compressive tectonic process and saturated with fluid/gas in the fractured zones (Italiano et al. 2013; Kop et al. 2014; Gulec and Hilton 2016). For instance, the fractured igneous rocks give rise to higher P-wave velocities, as saturation typically increases P-wave velocity. On the other hand, fracture accompanied by fluid saturation reduces the S-wave velocities, leading to a proportional increase in V_p/V_s values (Hauksson 2000; Kaypak 2008; Kaypak and Gokkaya 2012; Polat et al. 2016; Ozer et al. 2018).

Some studies claim that low P-wave velocity and low V_p/V_s ratios are found in gas-impregnated rocks, while low P-wave velocity and high V_p/V_s ratios are associated mainly with fluid-saturated, fractured and high-pore-pressure rocks such as dolomitic limestones, marbles, sandstones, ophiolitic melanges and evaporates (Hauksson 2000; Kaypak and Gokkaya 2012).

3.2.1 P-Velocity Model

The P-wave velocity model gives important information about the internal characteristics of different



◀Figure 10

Vertical V_p checkerboard test results for seven depth cross sections. The input depth cross sections (Fig. 10a) with block size of $30 \times 30 \text{ km}^2$ (with 5 km empty size) are applied to assess the stability of the vertical model. The tomographic results can be reliably interpreted according to the results of vertical checkerboard tests (Fig. 10b). The dashed lines indicate well-resolved areas. Periodic negative (blue) and positive (red) anomalies display $\pm 10\%$ velocity perturbations

geological layers. The inversion suggests four horizontal layers of seismic velocity structures beneath Eastern Anatolia: (1) the upper crust ($\sim 0\text{--}8 \text{ km}$, with $V_p \leq 4.6 \text{ km/s}$), (2) the middle crust ($\sim 8\text{--}20 \text{ km}$, with $4.6 < V_p \leq 5.8 \text{ km/s}$), (3) the lower crust ($\sim 20\text{--}35 \text{ km}$, with $5.8 < V_p \leq 7.4 \text{ km/s}$) and (4) the upper mantle layer (below 35 km, with $V_p > 7.4 \text{ km/s}$).

The upper crust layer ($\sim 0\text{--}8 \text{ km}$) Low P-wave velocity anomalies ($V_p \leq 4.0 \text{ km/s}$) are found along tectonic zones. It is clearly seen that V_p anomalies correlate with main geological characteristics and tectonic structures (Fig. 13). Low-velocity anomalies, on the other hand, follow the sedimentary basins and unconsolidated material deposits (Gok et al. 2007; Yusufoglu 2013; Kocuyigit and Canoglu 2017).

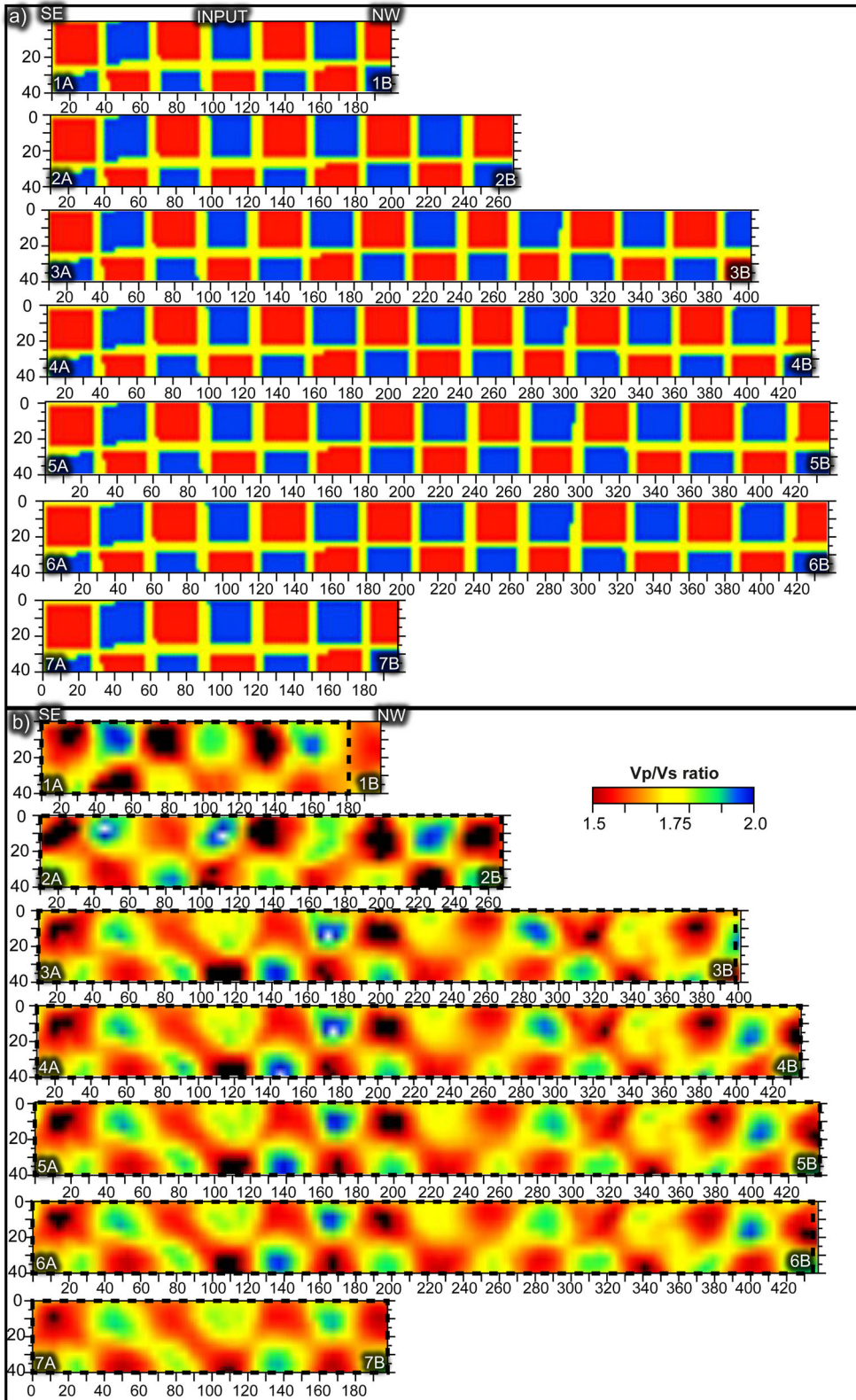
The middle crust layer ($\sim 8\text{--}20 \text{ km depth}$) The velocity characteristics of the middle crust layer compare to the upper crust layer, and a distinctive velocity feature is obvious at the middle-lower transmission at $\sim 20 \text{ km}$, known as the Conrad discontinuity (Fig. 13). It is evident that the well-resolved areas extend from 8 to 20 km, because of the hypocentre distribution (Fig. 4).

The lower crust layer ($\sim 20\text{--}35 \text{ km depth}$) Includes seismic velocities down to the upper mantle. The P-wave velocity in this layer ranges from 5.8 to 7.4 km/s. These velocities may also be related to the presence of volcanic units. Italiano et al. (2013) reported that the magnetic fluids were driven to the surface by lithospheric discontinuities along the EAFZ and that different lithologies might be impregnated with magma bodies, probably from the widespread Neogene-Quaternary volcanic activity in the upper crust (Fig. 13).

The upper mantle layer ($> 35 \text{ km depth}$) The high P-wave velocity ($V_p > 6.5 \text{ km/s}$) characteristics in the southward-dipping region is related to the subducting lithosphere. This high V_p zone is overlain

by a wedge-like body with V_p ranging between 7.4 and 9.0 km/s, representing the collided continental crust. The precise location of the Moho can be clearly seen in the tomogram (see also the even/odd and checkerboard test; Figs. 8, 9). Even though the stability of the tomographic computations at this depth is reduced, the Moho discontinuity can be deciphered from the undulated flat shape at $\sim 35 \text{ km}$. This depth is compatible with the conclusions of other studies using the receiver function method (Zor et al. 2003; Zor 2008; Salah et al. 2011; Bakirci et al. 2012; Sertcelik 2012; Vanacore et al. 2013; Tezel et al. 2013; Warren et al. 2013; Skolbeltsyn et al. 2014; Kind et al. 2015).

Low V_p velocities ($V_p \leq 4.0 \text{ km/s}$) were observed along the EAFZ and local faults (LF). Yusufoglu (2013) reported that regional compression occurred due to tectonic escape deformation between the Malatya-Adiyaman-Elazig triangle. They observed that the high seismic velocities ($V_p > 6.5 \text{ km/s}$) pointed to this escape and contacted upwards in profiles 2 and 3. Gok et al. (2007) claimed that low velocities ($V_p \leq 4.0 \text{ km/s}$) were associated with sedimentary units at depths of 2–4 km between longitudes 39.0–42.0 and latitudes 37.5–39.0. However, they also noted the sediment thickness of up to 7 km in the same study. These low velocities ($V_p \leq 4.0 \text{ km/s}$) can be observed along the EAFZ and BSZ at profiles 3, 4 and 5 (Fig. 13). Kocuyigit and Canoglu (2017) pointed out that no study had been conducted to reveal the geothermal potential of Erzurum and that the region had great potential in terms of hot water. In addition, geochemical studies carried out in the field of study show promising results, suggesting the presence of geothermal resources (Bayraktutan et al. 1996; Keskin et al. 2006; Yuce and Taskiran 2013; Italiano et al. 2013; Gulbay 2015; Kaygusuz et al. 2018). The V_p and V_p/V_s models along Erzurum and its surroundings are examined, and important indications can be traced. In particular, low V_p ($\leq 4.0 \text{ km/s}$) and high V_p/V_s (> 1.85) models are remarkable along local faults (Figs. 13, 14; profile 7). These anomalies support the notion that the region may be rich in terms of geothermal fluids, and much more work on a local scale should be planned. The obtained tomograms show that, except for profile 6, the Moho depth starts



◀Figure 11

Vertical V_p/V_s checkerboard test results for seven depth cross sections. The size of anomalies is $30 \times 30 \text{ km}^2$ with 5 km empty size (Fig. 11a). The tomographic results can be reliably interpreted according to the results of vertical V_p/V_s checkerboard tests (Fig. 11b). The dashed lines indicate well-resolved areas. V_p/V_s ratios range from 1.5 to 2.0

at 35 km and changes at a relatively flat rate. The tomographic sections coincide with the results reported by Gok et al. (2007, 2011). Profile 6 draws a different view from the other profiles. This is thought to be related to the tectonic compression regime, that the profile is cut by many local faults and located on the BSZ.

3.2.2 V_p/V_s Ratio Model

The V_p/V_s ratio indicates the mechanical and petrological properties of the crust. The low V_p/V_s ratio ($V_p/V_s \leq 1.65$) can relate to low V_p and low V_s

velocities (Fig. 14). The low value of the ratio is due to the fact that P-wave velocities are proportionally much lower than S-wave velocities, and thus the anomaly is generally associated with the presence of some type of gas (mostly CO_2). On the other hand, high values of the ratio ($V_p/V_s > 1.85$) are associated with low S-wave velocities, and they are interpreted as highly fractured, saturated rocks with high pore fluid pressure. This higher ratio can be used as an indicator of geothermal fluids (Dorbath and Granet 1996; Hauksson 2000; Kaypak 2008; Kaypak and Gokkaya 2012; Yolsal-Cevikbilen et al. 2012; Kuznetsov and Koulakov 2014; Ozer and Polat 2017b, c). Hence, there are two types of anomaly patterns, low and high V_p/V_s ratio.

Kaypak (2008) showed that the low V_p/V_s ratios were observed along the fault zones and could continue up to 10 km in Erzincan. Similarly, in all profiles except profile 7, low V_p/V_s ratios (V_p/V_s

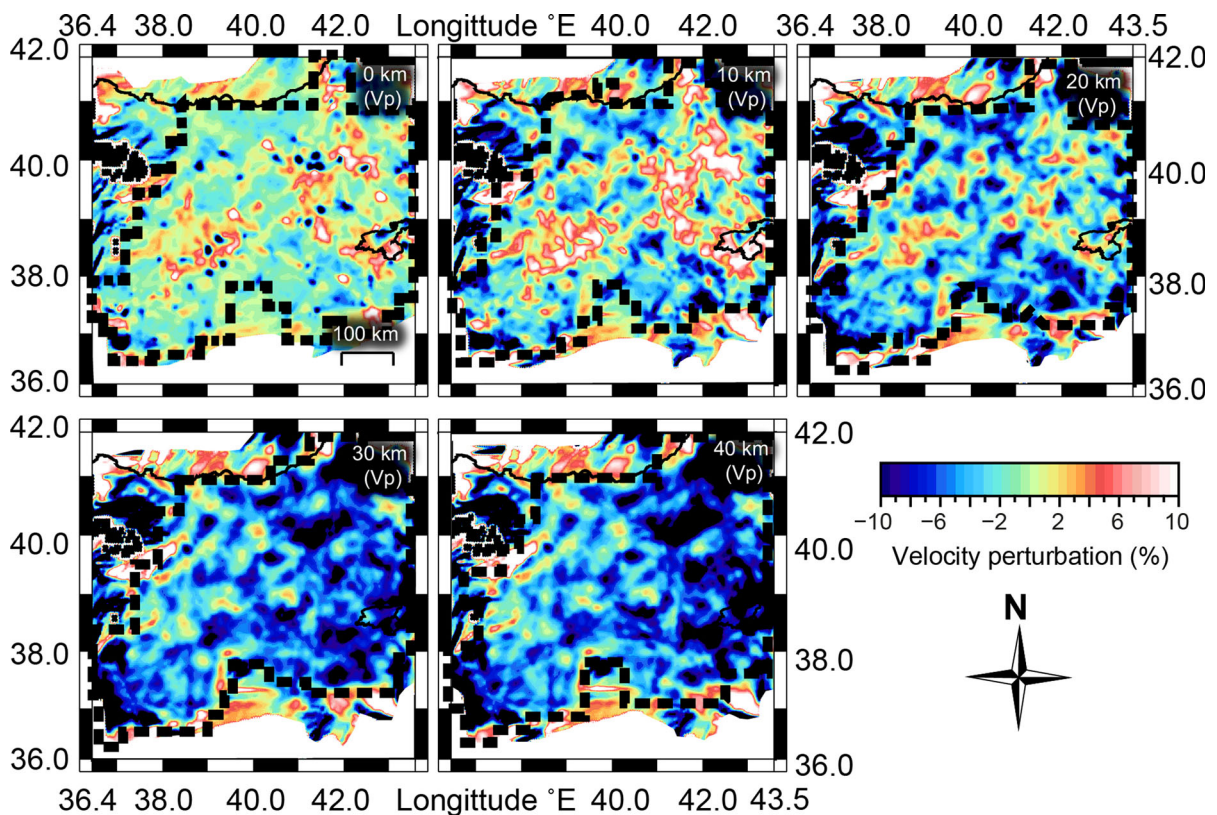
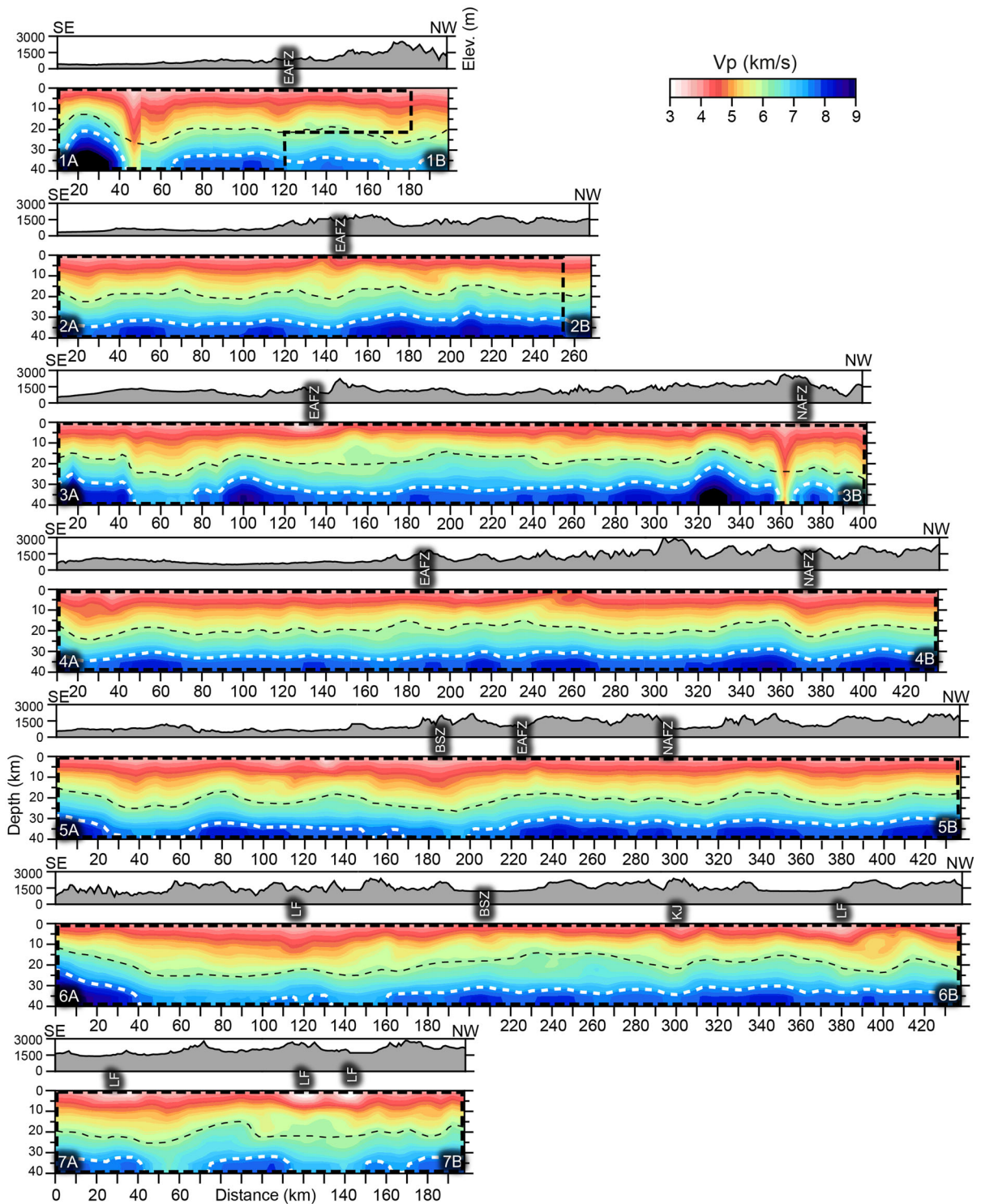


Figure 12

V_p tomographic horizontal section results for Eastern Anatolia. The dashed lines indicate well-resolved areas. Periodic negative (blue) and positive (red) anomalies display $\pm 10\%$ velocity perturbations



$V_s \leq 1.65$) were observed along the fault zones in this study. Some studies carried out in the area have reported that the area could contain hot water

(Italiano et al. 2013; Gulec and Hilton 2016; Kocyigit and Canoglu 2017). In profile 7, low V_p ($V_p \leq 4.0$ km/s) and high V_p/V_s ($V_p/V_s > 1.85$) ratios observed

◀Figure 13

Vertical sections of absolute P-wave velocity models. Locations of the profiles are presented in Fig. 2. Dashed thin black and white lines show approximate Conrad and Moho discontinuity depth, respectively. A detailed interpretation of low or high V_p/V_s ratios, along with V_p profiles, is given in the text. The thick black dashed lines indicate well-resolved areas. *LF* local fault

in Erzurum and its surroundings may indicate undiscovered hot water potential in the region (Fig. 14). For this reason, detailed local-scale studies are recommended in the study area.

4. Discussion

The V_p and the V_p/V_s ratio in particular are capable of portraying fault zones that operate to transport hot gas or fluid from deeper parts of the crust to the surficial layers in Eastern Anatolia. The results of other studies in the literature (Zor et al. 2003; Dolmaz et al. 2005; Bektas et al. 2007; Ozacar et al. 2008; Gokalp 2012; Bektas 2013), which use heat flow, Curie depth, receiver function, teleseismic tomography and microgravity measurements along the EAFZ, are in line with the V_p and V_p/V_s profiles obtained in this study.

Some prominent results from the above-mentioned studies are summarized in Fig. 15. Zor et al. (2003) point out the presence of a low S-wave velocity zone between 15 and 25 km, and report a tapering of crustal thickness based on the results of the V_p/V_s ratio in the region. They also discuss that the low-velocity zone may originate from younger basaltic volcanic rocks. In the southern part of the available Moho map, high seismic velocities are clearly visible at shallow depths, in concordance with the velocity characteristics in the first 40 km of the profiles in this study (Fig. 16). Bektas et al. (2007) give the depth of the brittle-ductile transition zone at around 20 km, which corresponds to the interface shown as the Conrad discontinuity in this study (Fig. 13). Pamukcu et al. (2007) emphasize that tectonics of Eastern Anatolia controlled by continent–continent collision and the thickness of the crust changes from 40 to 45 km. Ozacar et al. (2008) obtained a model of the crust (40 km) and the lithosphere (65 km) by the receiver

function method, and report that low velocities in the uppermost mantle create delays in arrival times. These results are coherent with the raised topography created by the partially molten and floating asthenosphere structure (Sengor et al. 2003). Zor (2008) studies the presence of upper mantle negative velocity perturbation values used to describe the uplift of the Eastern Anatolian Plateau. The slab-like high velocity along the Eastern Anatolia Accretionary Complex (EAAC) is interpreted as being a result of detached southern and northern slabs. Cambaz and Karabulut (2010) discuss the high volcanic activity from the upper Miocene to the Quaternary in Eastern Anatolia, and note that the Neo-Tethyan ocean floor was completely destroyed as a result of the collision of the Arabian and Eurasian plates during the Early Miocene. Therefore, high group velocities are normally observed in the Pontides and Bitlis-Poturge massif, which agrees well with our results. Salah et al. (2011) remark on the low P-velocities observed in the vicinity of the NAFZ, EAFZ, and the active volcanoes. In addition, most of the earthquake activity in the region is confined to the NAFZ and EAFZ. Some narrow zones with higher P-wave velocities are also observed, which suggests the presence of strain. In this region, earthquake activity is sparse. Bakirci et al. (2012) relate low seismic velocities to young Neogene and Holocene volcanism and claim that the Eastern Anatolian Plateau is under compression and has a weak structure as a subduction-accretion complex. They also report high seismic velocities beneath the subducting Arabian mantle lithosphere from the Zagros suture, substantiating our results in this study. Gokalp (2012) suggests that the high-velocity anomalies are related to remnants of the subducted lithosphere, which is partly responsible for the volcanism since the Late Miocene period, in eastern Turkey. Maden (2012) computes a temperature of 590 °C at a Moho depth of 35 km and shows the existence of a brittle-ductile zone. The Curie depth of 29 km, which can be associated with the crustal magma chambers, is found to be 5–7 km above the Moho depth. The high heat flow gradient in the mantle is likely related to melting of the lithospheric mantle, leading to upwelling of the asthenosphere. Bektas (2013) estimates the Moho depth in the region to vary between 33 and 37 km. The tomographic sections in

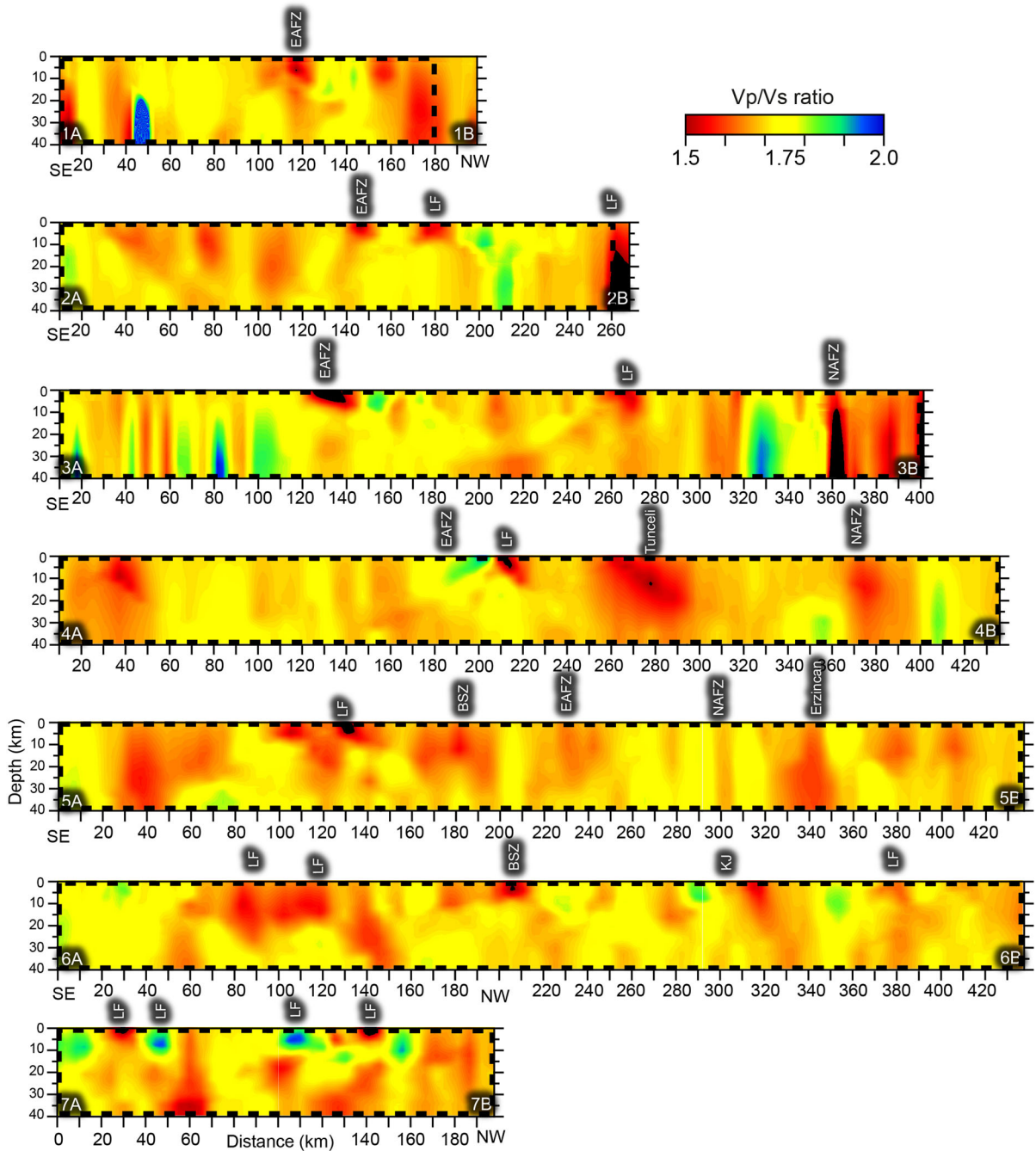


Figure 14

Vertical sections of V_p/V_s ratio models. Locations of the profiles are presented in Fig. 2. The thick black dashed lines indicate well-resolved areas

this study are compared with the magnetic, gravity, thermal structure and Curie depth values in the literature, which supports the notion that geothermal

systems in the region are associated with the current fault zones. Tezel et al. (2013) estimate a Moho depth of 40 km because of the high-altitude terrain in the

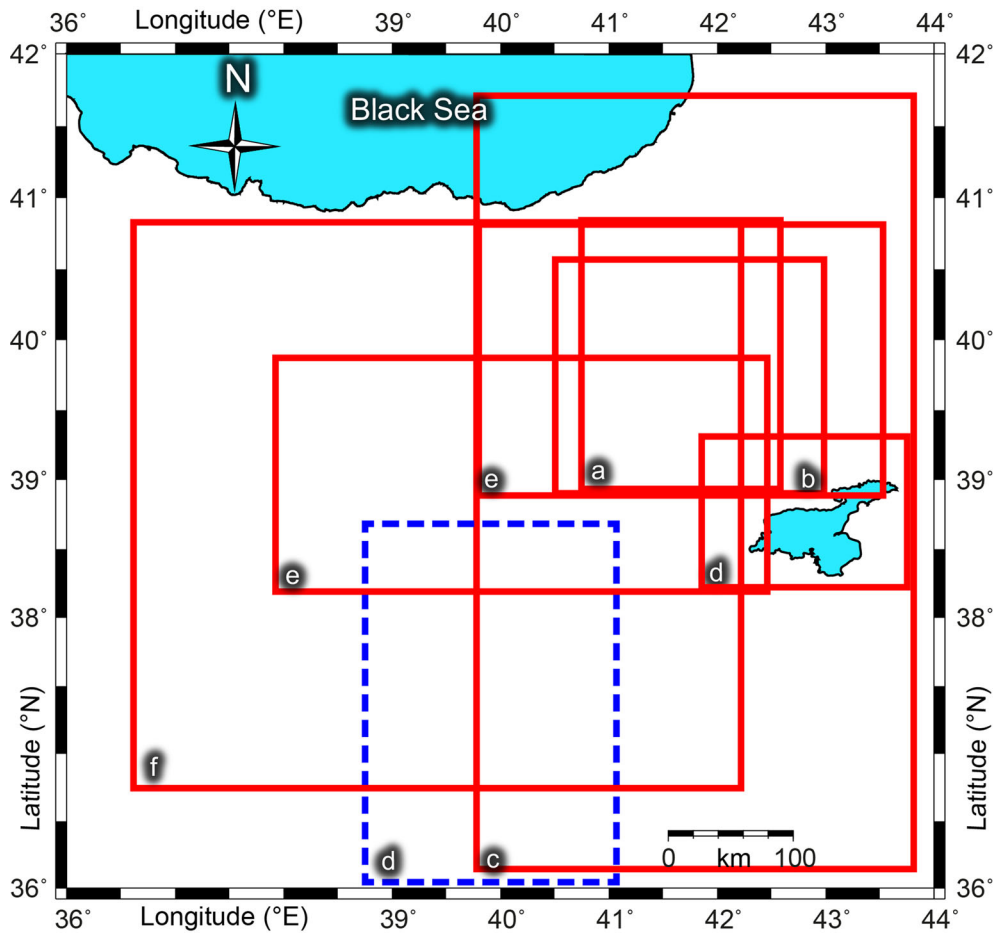


Figure 15

Summary view of notable tomographic studies previously performed in the study area: (a) Zor et al. (2003), (b) Ozacar et al. (2008), (c) Zor (2008), (d) Cambaz and Karabulut (2010), (e) Bakirci et al. (2012), and (f) this study

region and S-wave velocities of 4.1–4.4 km/s in the uppermost mantle. The low-velocity layer was calculated at 20–40 km depth. These results are associated with the Pontides, where the Eurasian and Arabian plate collision results in the volcanic arc and subduction in the region. Bartol and Govers' (2014) lithospheric model is also consistent with our tomograms for Eastern Anatolia. Skolbeltsyn et al. (2014) imaged the uppermost mantle structure in the Eastern Anatolian Region using surface wave tomography to display the regional tectonic structure of the collision between the Arabian and Eurasian plates. Their tomographic images enhance our understanding of the tectonic processes, which are responsible for the 2 km-high plateau and the volcanic activity in eastern

Turkey. The high-velocity values below the Arabian Plate, on the other hand, indicate cold lithospheric roots. The lack of a cold lithosphere in the model by Skolbeltsyn et al. (2014) is highly supportive of the existence of volcanism in the Arabian Plate. The positive S-wave perturbations beneath the EAAC may indicate a delaminated block of lithosphere. The authors propose that this high-velocity body is another piece of the broken-off Bitlis slab, probably the shallowest part of the slab. In Maden et al. (2015), the Moho, Conrad and sediment depths are computed as 43 km, 20.9 km and 5.2 km, respectively. The high heat flow values are likely associated with the crustal magma chambers and the ophiolitic and young volcanic rocks covering a large area in Eastern Anatolia.

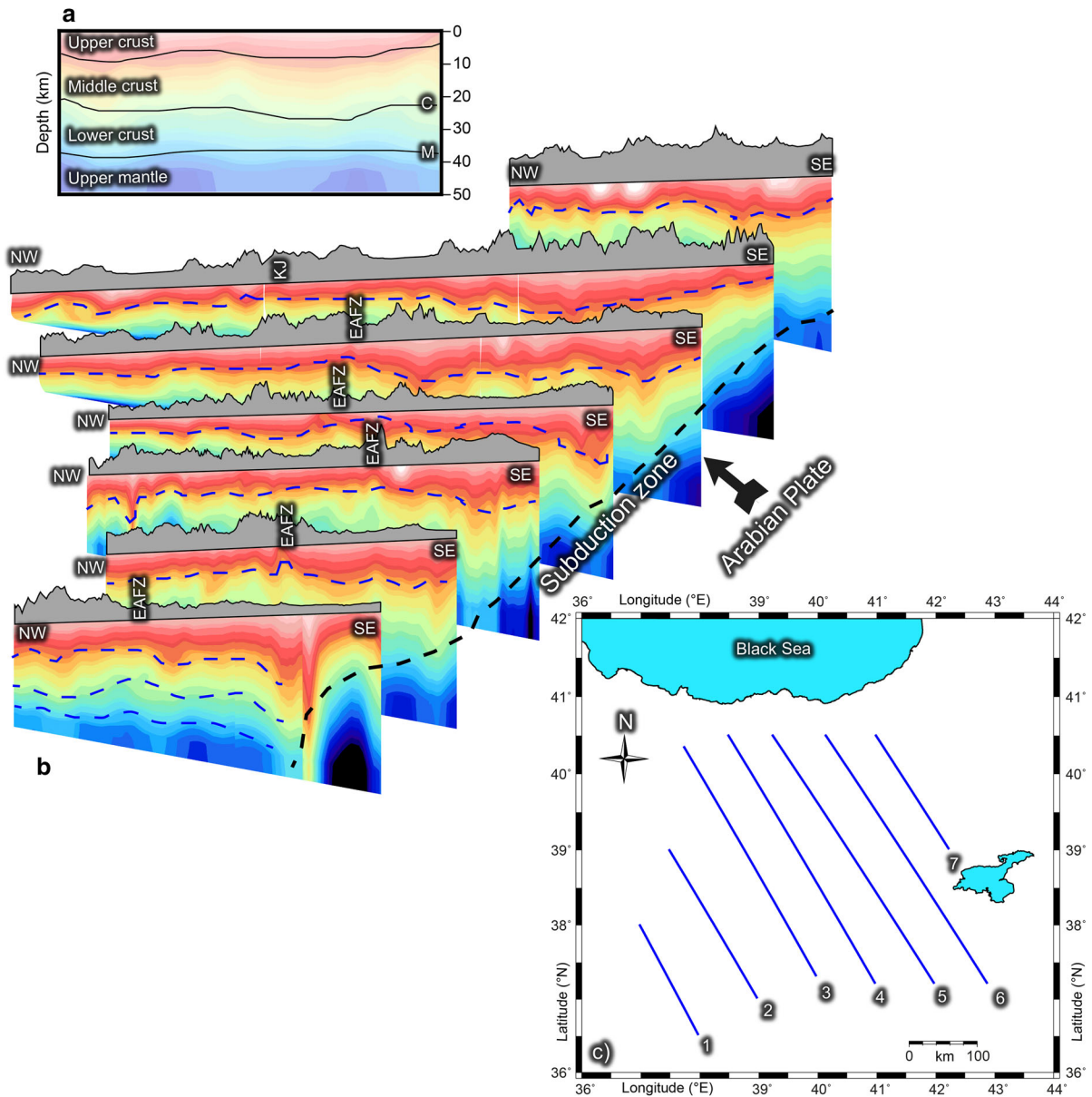


Figure 16

Conceptual cartoon beneath Eastern Anatolia along the SE–NW direction based on the P-wave structure. **a** Border of seismic structures indicating four main seismic layers are shown schematically. **b** The predicted seismic layer boundaries are shown as blue dashed lines. Color palette of V_p , same as in Fig. 13. Subduction zone boundaries are shown as black dashed lines. **c** Conrad discontinuity, EAFZ East Anatolian Fault Zone, KJ Karliova junction, M Moho discontinuity. **c** The location of the seven vertical depth cross sections

Hence, the high heat flow values can also be related to the melting of the lithospheric mantle owing to the elevating asthenosphere. Turkoglu et al. (2015) note that the measured low resistivity (high conductivity)

values are an indicator of fluid content along the EAFZ. All of these results are consistent with the tomographic images developed in this study, as seen in all depth cross sections.

In this study, the EAFZ is investigated at a regional scale and interpreted in detail. Figure 16 providing a summary of the study is given in Gok et al. (2007) and Skolbeltsyn et al. (2014), and is consistent with the schematic diagram of the N–S direction plot. Our tomographic images open up a new perspective for the Eastern Anatolian crustal structure, as shown by the summary model in Fig. 16. We propose high-velocity zones beneath the subduction zone, as illustrated in V_p seismic depth cross sections (Fig. 16b). The zones/structures with high-velocity intrusion from the upper mantle to the upper crust observed at lower levels of almost all seismic layers probably indicate a thrust fault zone extending from deeper parts up to 10 km. The relative motion of the Arabian and Anatolian plates is clearly detectable from the high V_p velocities. It is found that the average crustal P-wave velocity profile in Eastern Anatolia divides the region into four seismic zones (Fig. 16a). In addition, the Conrad and Moho discontinuities are computed at depths of ~ 20 km and ~ 35 km, respectively (Fig. 16c).

5. Conclusions

This study presents a new local earthquake tomography application in Eastern Anatolia and provides an important perspective regarding the tectonic process in the region, suggesting the presence of some clandestine reservoirs that have not yet been investigated. P-wave velocity and V_p/V_s ratio profiles present important knowledge about the lithological and petrological structure of the study area. The seismic velocity values of the East Anatolian Fault Zone, which presents the tomographic results of the P-wave and V_p/V_s ratio, coincide with the geological and tectonic structure. Using the data from 78 stations, operated by AFAD, 4249 earthquakes are selected for this study. Seven depth cross sections (V_p and V_p/V_s) were created along the SE and NW directions to evaluate and display seismic velocity characteristics beneath some potential geothermal areas and the subduction zone. The variations in the V_p and V_p/V_s ratio in eastern Turkey are tomographically mapped down to a depth of 40 km. P-wave velocities and V_p/V_s ratio vary from 3.0 to 9.0 km/s

and from 1.5 to 2.0, respectively. We propose a four-layer seismic model of the crustal structure beneath the Eastern Anatolia: the upper crust (~ 0 –8 km depth, $V_p \leq 4.6$ km/s), middle crust (~ 8 –20 km depth, $4.6 < V_p \leq 5.8$ km/s), lower crust (~ 20 –35 km depth, $5.8 < V_p \leq 7.4$ km/s) and upper mantle layer (> 35 km depth, $V_p > 7.4$ km/s). The positive P-wave velocity values in the horizontal section along the EAFZ on the surface are associated with volcanic and ophiolite units. It is thought that the negative velocity changes observed in deep parts are due to the hot mantle effect which is related to volcanism. The high seismic velocities ($V_p > 6.5$ km/s) which are believed to be caused by the regional compression effect depending on the tectonic escape deformation, make contact from the deep parts to the surface. In particular, the high V_p velocities ($V_p > 6.5$ km/s) that make contact in the southeast are associated with the subduction zone resulting from the compression of the Arabian and Anatolian plates. This study estimates the seismogenic depth to vary from 0 to 20 km, with the Conrad discontinuity at 20 km. The average Moho depth is estimated at around 35 km. Furthermore, low V_p ($V_p \leq 4.0$ km/s) and high V_p/V_s ($V_p/V_s > 1.85$) models increase the likelihood that the region may be rich in geothermal resources transported by local faults for Erzurum and its surroundings. Additional local magnetotellurics (MT), seismic and gravity measurements are needed to determine whether the fault zone fluid content controls the seismic characteristics or whether the fluids are deployed only as a result of the deformation process.

Acknowledgements

This study is supported by the 2016.KB.FEN.013 project, and the data are provided by AFAD (Ankara-Turkey). We are grateful to the editor, Colin Farquharson, for his fruitful and constructive criticisms, as well as anonymous reviewers for their critical remarks, which helped us to improve the paper. LOTOS code is used in developing the tomograms. All images are created using GMT (Wessel et al. 2013). Faults are digitized in the Geoscience map viewer (Emre et al. 2013) and

drawing editor licensed to the General Directorate of Mineral Research and Exploration (MTA). The data are collected in SEISAN (Havskov and Ottemoller 1999) software.

Publisher's Note Springer Nature remains neutral with regard to jurisdictional claims in published maps and institutional affiliations.

REFERENCES

- Aksu, A. E., Calon, T. J., Piper, D. J. W., Turgut, S., & Izdar, E. (1992). Architecture of late orogenic Quaternary basins in northeastern Mediterranean Sea. *Tectonophysics*, *210*, 191–213.
- Aktug, B., Ozener, H., Dogru, A., Sabuncu, A., Turgut, B., Haliçioğlu, K., et al. (2016). Slip rates and seismic potential on the East Anatolian Fault System using an improved GPS velocity field. *Journal of Geodynamics*, *94–95*, 1–12.
- Bakirci, T., Yoshizawa, K., & Ozer, M. F. (2012). Three-dimensional S-wave structure of the upper mantle beneath Turkey from surface wave tomography. *Geophysical Journal International*, *190*(2), 1058–1076.
- Bartol, J., & Govers, R. (2014). A single cause for uplift of the Central and Eastern Anatolian plateau? *Tectonophysics*, *637*, 116–136.
- Bayraktutan, M. S., Merefield, J. R., Grainger, P., Evans, B. M., Yilmaz, M., & Kalkan, E. (1996). Regional gas geochemistry in an active tectonic zone, Erzurum basin, eastern Turkey. *Quarterly Journal of Engineering Geology*, *29*(3), 209–218.
- Bektas, O. (2013). Thermal structure of the crust in Inner East Anatolia from aeromagnetic and gravity data. *Physics of the Earth and Planetary Interiors*, *221*, 27–37.
- Bektas, O., Ravat, D., Buyuksarac, A., Bilim, F., & Ates, A. (2007). Regional geothermal characterisation of East Anatolia from aeromagnetic, heat flow and gravity data. *Pure and Applied Geophysics*, *164*(5), 975–998.
- Burke, K., & Sengor, A. M. C. (1986). Tectonic escape in the evolution of the continental crust. In M. Barazangi & L. Brown (Eds.), *Reflection seismology: The continental crust* (pp. 41–53). Washington: Geophysical Union.
- Cambaz, M. D., & Karabulut, H. (2010). Love-wave group velocity maps of Turkey and surrounding regions. *Geophysical Journal International*, *181*(1), 502–520.
- Cetin, H., Güneçli, H., & Mayer, L. (2003). Paleoseismology of the Palu-Lake Hazar segment of the East Anatolian Fault Zone, Turkey. *Tectonophysics*, *374*(3), 163–197.
- Delph, J. R., Biryol, C. B., Beck, S. L., Zandt, G., & Ward, K. M. (2015). Shear wave velocity structure of the Anatolian Plate: Anomalous slow crust in southwestern Turkey. *Geophysical Journal International*, *202*, 261–276.
- Dewey, J. F., Hempton, M. R., Kidd, W. S. F., Saroglu, F., & Sengor, A. M. C. (1986). Shortening of continental lithosphere: The neo-tectonics of eastern Anatolia—a young collision zone. In M. P. Coward & A. C. Reis (Eds.), *Collision tectonics* (pp. 3–36). London: Geological Society.
- Dinc, A. N., Koulakov, I., Thorwart, M., Rabbal, W., Fluesh, E. R., Arroyo, I., et al. (2010). Local earthquake tomography of central Costa Rica: Transition from seamount to ridge subduction. *Geophysical Journal International*, *183*(1), 286–302.
- Dolmaz, N. M., Elitok, O., & Kalyoncuoglu, U. Y. (2008). Interpretation of low seismicity in the Eastern Anatolian collisional zone using geophysical (seismicity and aeromagnetic) and geological data. *Pure and Applied Geophysics*, *165*, 311–330.
- Dolmaz, M. N., Ustaomer, T., Hisarli, Z. M., & Orbay, N. (2005). Curie Point Depth variations to infer thermal structure of the crust at the African-Eurasian convergence zone, SW Turkey. *Earth Planets Space*, *57*, 373–383.
- Dorbath, C., & Granet, M. (1996). Local earthquake tomography of the Altiplano and the Eastern Cordillera of northern Bolivia. *Tectonophysics*, *259*(1–3), 117–136.
- Duman, T. Y., & Emre, O. (2013). The East Anatolian Fault: Geometry, segmentation and jog characteristics. *Geological Society Special Publications*, *372*(1), 495–529.
- Emre, O., Duman, T. Y., Ozalp, S., Elmaci, H., Olgun, S., & Saroglu, F. (2013). 1/1.125.000 Ölçekli Türkiye Diri Fay Haritası. Maden Tetkik ve Arama Genel Müdürlüğü Özel Yayınlar Serisi, Ankara. <http://www.mta.gov.tr/v3.0/>. Accessed 19 June 2018.
- Ergin, M., Aktar, M., & Eyidogan, H. (2004). Present-day seismicity and seismotectonics of the Cilician basin: Eastern Mediterranean region of Turkey. *Bulletin of the Seismological Society of America*, *94*(3), 930–939.
- Gentile, G., Bressan, G., Burlini, L., & De Franco, R. (2000). Three dimensional V_p and V_p/V_s models of the upper-crust in the Friuli area (northeastern Italy). *Geophysical Journal International*, *141*, 457–478.
- Gok, R., Mahdi, H., Al-Shukri, H., & Rodgers, A. J. (2008). Crustal structure of Iraq from receiver functions and surface wave dispersion: Implications for understanding the deformation history of the Arabian-Eurasian collision. *Geophysical Journal International*, *172*, 1179–1187.
- Gok, R., Mellors, R. J., Sandvol, E., Pasyanos, M., Hauk, T., Takedatsu, R., et al. (2011). Lithospheric velocity structure of the Anatolian plateau-Caucasus-Caspian region. *Journal of Geophysical Research*, *116*, B05303.
- Gok, R., Pasyanos, M. E., & Zor, E. (2007). Lithospheric structure of the continent-continent collision zone: Eastern Turkey. *Geophysical Journal International*, *169*(3), 1079–1088.
- Gok, R., Sandvol, E., Turkelli, N., Seber, D., & Barazangi, M. (2003). Sn attenuation in the Anatolian and Iranian plateau and surrounding regions. *Geophysical Research Letters*, *30*(24), 8042.
- Gokalp, H. (2007). Local earthquake tomography of the Erzincan Basin and the surrounding area in Turkey. *Annals of Geophysics*, *50*(6), 707–724.
- Gokalp, H. (2012). Tomographic Imaging of the Seismic Structure beneath the East Anatolian Plateau, Eastern Turkey. *Pure and Applied Geophysics*, *169*(10), 1749–1776.
- Gulbay, R. K. (2015). Organic geochemical and petrographical characteristics of coal bearing Oligo-Miocene sequence in the Oltu-Narman Basin (Erzurum), NE Turkey. *International Journal of Coal Geology*, *149*(1), 93–107.
- Gulec, N., & Hilton, D. R. (2016). Turkish geothermal fields as natural analogues of CO₂ storage sites: Gas geochemistry and implications for CO₂ trapping mechanisms. *Geothermics*, *64*, 96–110.

- Gursoy, H., Tatar, O., Piper, J. D. A., Heimann, A., & Mesci, L. (2003). Neotectonic deformation linking the East Anatolian and Karatas-Osmaniye intracontinental transform fault zones in the Gulf of Iskenderun, southern Turkey, deduced from paleomagnetic study of the Ceyhan-Osmaniye volcanics. *Tectonics*, 22(6), 1067.
- Hauksson, E. (2000). Crustal structure and seismicity distribution adjacent to the Pacific and North America plate boundary in southern California. *Journal of Geophysical Research*, 105, 13875.
- Havskov, J., & Ottemoller, L. (1999). SeisAn Earthquake analysis software. *Seismological Research Letters*, 70(55), 532–534.
- Hempton, M. R. (1985). Structure and deformation history of the Bitlis suture near Lake Hazar, southeastern Turkey. *Geological Society of America Bulletin*, 96, 233–243.
- Hempton, M. R. (1987). Constraints on Arabian plate motion and extensional history of the Red Sea. *Tectonics*, 6, 687–705.
- Hempton, M. R., Dewey, J. F., & Saroglu, F. (1981). The East Anatolian transform fault: Along strike variations in geometry and behaviour. *Eos Transactions American Geophysical Union*, 62, 393.
- Italiano, F., Sasmaz, A., Yuce, G., & Okan, O. O. (2013). Thermal fluids along the East Anatolian Fault Zone (EAFZ): Geochemical features and relationships with the tectonic setting. *Chemical Geology*, 339, 103–114.
- Jackson, J. (1994). Active tectonics of the Aegean region. *Annual Review of Earth and Planetary Sciences*, 22, 239–271.
- Jaxybulatov, K., Koulakov, I., Seht, M., Klinge, K., Reichert, B. D., & Troll, V. R. (2011). Evidence for high fluid/melt content beneath Krakatau volcano (Indonesia) from local earthquake tomography. *Journal of Volcanology and Geothermal Research*, 206(3–4), 96–105.
- Kaygusuz, A., Aslan, Z., Aydınçakır, E., Yücel, C., Gücer, M. A., & Şen, C. (2018). Geochemical and Sr-Nd-Pb isotope characteristics of the Miocene to Pliocene volcanic rocks from the Kandilli (Erzurum) area, Eastern Anatolia (Turkey): Implications for magma evolution in extension-related origin. *Lithos*, 296, 332–351.
- Kaypak, B. (2008). Three-dimensional VP and VP/VS structure of the upper crust in the Erzincan basin (eastern Turkey). *Journal of Geophysical Research: Solid Earth*, 113(7), 20.
- Kaypak, B., & Eyidogan, H. (2005). One-dimensional crustal structure of the Erzincan basin, Eastern Turkey and relocations of the 1992 Erzincan earthquake ($M_s = 6.8$) aftershock sequence. *Physics of the Earth and Planetary Interiors*, 151(1–2), 1–20.
- Kaypak, B., & Gokkaya, G. (2012). 3-D imaging of the upper crust beneath the Denizli geothermal region by local earthquake tomography, western Turkey. *Journal of Volcanology and Geothermal Research*, 211–212, 47–60.
- Keskin, M., Pearce, J. A., Kempton, P. D., & Greenwood, P. (2006). Magma-crust interactions and magma plumbing in a post-collisional setting: Geochemical evidence from the Erzurum-Kars volcanic plateau, eastern Turkey. *Geological Society of America Special Paper*, 409, 475–505.
- Khrepy, S., Koulakov, I., & Al-Arifi, N. (2015). Crustal structure in the area of the cannon earthquakes of Abu Dabbab (northern Red Sea, Egypt), from seismic tomography inversion. *Bulletin of the Seismological Society of America*, 105(4), 1870–1882.
- Kilic, T., Ottemoller, L., Havskov, J., Yanik, K., Kilicarslan, O., Alver, F., et al. (2017). Local magnitude scale for earthquakes in Turkey. *Journal of Seismology*, 21(1), 35–46.
- Kind, R., Eken, T., Tilmann, F., Sodoudi, F., Taymaz, T., Bulut, F., et al. (2015). Thickness of the lithosphere beneath Turkey and surroundings from S-receiver functions. *Solid Earth*, 6, 971–984.
- Kocycigit, A., & Canoglu, M. C. (2017). Neotectonics and seismicity of Erzurum pull-apart basin, East Turkey. *Russian Geology and Geophysics*, 58, 99–122.
- Kop, A., Ezer, M., Bodur, M. N., Darbas, G., Inan, S., Ergintav, S., et al. (2014). Geochemical Monitoring Along the Turkoglu (Kahramanmaraş)-Golbasi (Adiyaman) Segments of the East Anatolian Fault System. *Arabian Journal for Science and Engineering*, 39(7), 5521–5536.
- Koulakov, I. (2009). LOTOS code for local earthquake tomographic inversion: Benchmarks for testing tomographic algorithms. *Bulletin of the Seismological Society of America*, 99(1), 194–214.
- Koulakov, I., Sobolev, S. V. (2006). Moho depth and three-dimensional and structure of the crust and uppermost mantle in the Eastern Mediterranean and Middle East derived from tomographic inversion of local ISC data. *Geophysical Journal International*, 164(1), 218–235.
- Koulakov, I., Jakovlev, A., & Luehr, B. G. (2009). Anisotropic structure beneath central Java from local earthquake tomography. *Geochem Geophys Geosyst*, 10(2), Q02011.
- Koulakov, I., Zaharia, B., Enescu, B., Radulian, M., Popa, M., Parolai, S., et al. (2010). Delamination or slab detachment beneath Vrancea? New arguments from local earthquake tomography. *Geochem Geophys Geosyst*, 11(3), Q03002.
- Kuznetsov, P. Y., & Koulakov, I. (2014). The three-dimensional structure beneath the Popocatepetl volcano (Mexico) based on local earthquake seismic tomography. *Journal of Volcanology and Geothermal Research*, 276, 10–21.
- Le Pichon, X., Chamot-Rooke, N., & Lallemand, S. (1995). Geodetic determination of the kinematics of central Greece with respect to Europe: Implications for eastern Mediterranean tectonics. *Journal of Geophysical Research*, 100, 12,675–12,690.
- Le Pichon, X., & Kreemer, C. (2010). The Miocene-to-present kinematic evolution of the Eastern Mediterranean and Middle East and its implications for dynamics. *Annual Review of Earth and Planetary Sciences*, 38(1), 323–351.
- Maden, N. (2012). One-dimensional thermal modeling of the Eastern Pontides Orogenic Belt (NE Turkey). *Pure and Applied Geophysics*, 169(1), 235–248.
- Maden, N., Aydin, A., & Kadirov, F. (2015). Determination of the crustal and thermal structure of the Erzurum-Horasan-Pasinler Basins (Eastern Turkey) using gravity and magnetic data. *Pure and Applied Geophysics*, 172(6), 1599–1614.
- McClusky, S., Balassanian, S., Barka, A., Demir, C., Ergintav, S., Georgiev, I., et al. (2000). Global Positioning System constraints on plate kinematics and dynamics in the eastern Mediterranean and Caucasus. *Journal of Geophysical Research*, 105, 5695–5719.
- McKenzie, D. (1972). Active tectonics of the Mediterranean Region. *Geophysical Journal International*, 30, 109–185.

- McKenzie, D. (1976). The east Anatolian fault: A major structure in eastern Turkey. *Earth and Planetary Science Letters*, 29, 189–193.
- Mutlu, A. K., & Karabulut, H. (2011). Anisotropic Pn tomography of Turkey and adjacent regions. *Geophysical Journal International*, 187(3), 1743–1758.
- Nalbant, S. S., McCloskey, J., Steacy, S., & Barka, A. A. (2002). Stress accumulation and increased seismic risk in eastern Turkey. *Earth and Planetary Science Letters*, 195(3–4), 291–298.
- Orgulu, G., Aktar, M., Turkelli, N., Sandvol, E., & Barazangi, M. (2003). Contribution to the seismotectonics of Eastern Turkey from moderate and small size events. *Geophysical Research Letters*, 30(24), 8040.
- Ozacar, A. A., Gilbert, H., & Zandt, G. (2008). Upper mantle discontinuity structure beneath East Anatolian Plateau (Turkey) from receiver functions. *Earth and Planetary Science Letters*, 269(3–4), 426–434.
- Ozer, C., Gok, E., & Polat, O. (2018). Three-dimensional seismic velocity structure of the Aegean Region of Turkey from local earthquake tomography. *Annals of Geophysics*, 61(1), 1–21.
- Ozer, C., & Polat, O. (2017a). Determination of 1-D (One-Dimensional) seismic velocity structure of Izmir and surroundings. *Journal of Science and Engineering*, 19, 147–168. <https://doi.org/10.21205/deufmd.2017195512>.
- Ozer, C., & Polat, O. (2017b). Local earthquake tomography of Izmir geothermal area, Aegean region of Turkey. *Bollettino di Geofisica Teorica ed Applicata*, 58(1), 17–42.
- Ozer, C., & Polat, O. (2017c). 3-D crustal velocity structure of Izmir and surroundings. *Journal of the Faculty of Engineering and Architecture of Gazi University*, 32(3), 733–747.
- Paige, C. C., & Saunders, M. (1982). LSQR: An algorithm for sparse linear equations and sparse least squares. *ACM Transactions on Mathematical Software*, 8(1), 43–71.
- Pamukcu, O. A., Akcig, Z., Demirbas, S., & Zor, E. (2007). Investigation of crustal thickness in Eastern Anatolia using gravity, magnetic and topographic data. *Pure and Applied Geophysics*, 164(11), 2345–2358.
- Perincek, D., & Cemen, I. (1990). The structural relationship between the East Anatolian and Dead Sea fault zones in south-eastern Turkey. *Tectonophysics*, 172, 331–340.
- Polat, G., Ozel, N. M., & Koulakov, I. (2016). Investigating P- and S-wave velocity structure beneath the Marmara region (Turkey) and the surrounding area from local earthquake tomography. *Earth, Planets and Space*, 68(132), 1–14.
- Reilinger, R., McClusky, S., Vernant, P., Lawrence, S., Ergintav, S., Cakmak, R., et al. (2006). GPS constraints on continental deformation in the Africa-Arabia-Eurasia continental collision zone and implications for the dynamics of plate interactions. *Journal of Geophysical Research, Solid Earth*, 111(B5), B05411.
- Salah, M. H. (2014). Upper crustal structure beneath Southwest Iberia north of the convergent boundary between the Eurasian and African plates. *Geoscience Frontiers*, 5(6), 845–854.
- Salah, M. K., Sahin, S., & Aydin, U. (2011). Seismic velocity and Poisson's ratio tomography of the crust beneath East Anatolia. *Journal of Asian Earth Sciences*, 40(3), 746–761.
- Sandvol, E., Turkelli, N., & Barazangi, M. (2003). The Eastern Turkey Seismic Experiment: The study of a young continent-continent collision. *Geophysical Research Letters*, 30(24), 8038.
- Saroglu, F., Emre, O., & Kusu, I. (1992). The East Anatolian fault zone of Turkey. *Annales Tectonicae*, 6, 99–125.
- Sengor, A. M. C., & Natal'in, B. A. (1996). Turcic-type orogeny and its role in the making of the continental crust. *Annual Review of Earth and Planetary Sciences*, 24, 263–337.
- Sengor, A. M. C., Ozeren, S., Genc, T., & Zor, E. (2003). East Anatolian high plateau as a mantle-supported, north-south shortened domal structure. *Geophysical Research Letters*, 30(24), 2–5.
- Serrano, I., Zhao, D., & Morales, J. (2002). 3-D crustal structure of the extensional Granada Basin in the convergent boundary between the Eurasian and African plates. *Tectonophysics*, 344(1–2), 61–79.
- Sertcelik, F. (2012). Estimation of coda wave attenuation in the East Anatolia fault zone, Turkey. *Pure and Applied Geophysics*, 169(7), 1189–1204.
- Simao, N. M., Nalbant, S. S., Sunbul, F., & Mutlu, A. K. (2016). Central and eastern Anatolian crustal deformation rate and velocity fields derived from GPS and earthquake data. *Earth and Planetary Science Letters*, 433, 89–98.
- Skolbeltsyn, G., Mellors, R., Gok, R., Turkelli, N., Yetirmishli, G., & Sandvol, E. (2014). Upper mantle S wave velocity structure of the East Anatolian-Caucasus region. *Tectonics*, 33(3), 207–221.
- Teoman, U. M., Turkelli, N., Gok, R. (2005). Dogu Anadolu Bolgesi Ust Kabuk Hiz Yapisinin Uc-Boyutlu Yerel Deprem Tomografisi Yontemi ile Belirlenmesi. http://kocaeli2007.kocaeli.edu.tr/kocaeli2005/deprem_sempozyumu_kocaeli_2005/2_yer_yapisi/d_11_kabuk_yapisi_calismalari/dogu_anadolu_bolgesi_ust_kabuk_hiz_yapisinin_uc_boyutlu.pdf. Accessed 29 June 2018.
- Tezel, T., Shibutani, T., & Kaypak, B. (2013). Crustal thickness of Turkey determined by receiver function. *Journal of Asian Earth Sciences*, 75, 36–45.
- Totaro, C., Koulakov, I., Orecchio, B., & Presti, D. (2014). Detailed crustal structure in the area of the southern Apennines-Calabrian Arc border from local earthquake tomography. *Journal of Geodynamics*, 82, 87–97.
- Turkoglu, E., Unsworth, M., Bulut, F., & Caglar, I. (2015). Crustal structure of the North Anatolian and East Anatolian Fault Systems from magnetotelluric data. *Physics of the Earth and Planetary Interiors*, 241, 1–14.
- Vanacore, E. A., Taymaz, T., & Saygin, E. (2013). Moho structure of the Anatolian plate from receiver function analysis. *Geophysical Journal International*, 193(1), 329–337.
- Wagner, D., Koulakov, I., Rabbel, W., Luehr, B. G., Wittwer, A., Kopp, H., et al. (2007). Joint inversion of active and passive seismic data in Central Java. *Geophysical Journal International*, 170(2), 923–932.
- Walters, R. J., Parsons, B., & Wright, T. J. (2014). Constraining crustal velocity fields with InSAR for Eastern Turkey: Limits to the block-like behavior of Eastern Anatolia. *Journal of Geophysical Research, Solid Earth*, 119(6), 5215–5234.
- Warren, L. M., Beck, S. L., Biryol, C. B., Zandt, G., Ozacar, A. A., & Yang, Y. (2013). Crustal velocity structure of Central and Eastern Turkey from ambient noise tomography. *Geophysical Journal International*, 194(3), 1941–1954.
- Wessel, P., Smith, W. H. F., Scharroo, R., Luis, J. F., & Wobbe, F. (2013). Generic Mapping Tools: Improved version released. *EOS Transactions American Geophysical Union*, 94, 409–410.
- Yolsal-Cevikbilen, S., Biryol, C. B., Beck, S., Zandt, G., Taymaz, T., Adiyaman, H. E., et al. (2012). 3-D crustal structure along the North Anatolian Fault Zone in north-central Anatolia revealed by

- local earthquake tomography. *Geophysical Journal International*, 188(3), 819–849.
- Yuce, G., & Taskiran, L. (2013). Isotope and chemical compositions of thermal fluids at Tekman Geothermal Area (Eastern Turkey). *Geochemical Journal*, 47, 423–435.
- Yusufoglu, H. (2013). An intramontane pull-apart basin in tectonic escape deformation: Elbistan Basin, Eastern Taurides, Turkey. *Journal of Geodynamics*, 65, 308–329.
- Zor, E. (2008). Tomographic evidence of slab detachment beneath eastern Turkey and the Caucasus. *Geophysical Journal International*, 175(3), 1273–1282.
- Zor, E., Sandvol, E., Gurbuz, C., Turkelli, N., Seber, D., & Barazangi, M. (2003). The crustal structure of the East Anatolian plateau (Turkey) from receiver functions. *Geophysical Research Letters*, 30(24), 8044.

(Received May 4, 2018, revised December 5, 2018, accepted December 7, 2018, Published online December 17, 2018)